

UNCLASSIFIED

AD NUMBER
AD003294
NEW LIMITATION CHANGE
TO Approved for public release, distribution unlimited
FROM Distribution: No Foreign.
AUTHORITY
AFAL ltr., 17 Aug 1979

THIS PAGE IS UNCLASSIFIED

62-10501003

53-9-22077

DO NOT DESTROY
RETURN TO
TECHNICAL EQUIPMENT
CONTROL SECTION
WFO:AS

TL 4029

WADC TECHNICAL REPORT 52-227

FILE COPY

RECEIVED BY
AS AD 110-22-94

**PROPERTIES OF TEMPERATURE-RESISTANT MATERIALS
UNDER TENSILE AND COMPRESSIVE FATIGUE STRESS**

B. J. LAZAN
E. WESTBERG

SYRACUSE UNIVERSITY

NOVEMBER 1952

WRIGHT AIR DEVELOPMENT CENTER

PLEASE RETURN TO:

ARMED SERVICES TECHNICAL INFORMATION AGENCY
DOCUMENT SERVICE CENTER
Knott Building, Dayton 2, Ohio

Because of our limited supply you are requested to return
this copy as soon as it has served your purposes so that
it may be made available to others for reference use.
cooperation will be appreciated.

20010501003

NOTICES

When Government drawings, specifications, or other data are used for any purpose other than in connection with a definitely related Government procurement operation, the United States Government thereby incurs no responsibility nor any obligation whatsoever; and the fact that the Government may have formulated, furnished, or in any way supplied the said drawings, specifications, or other data, is not to be regarded by implication or otherwise as in any manner licensing the holder or any other person or corporation, or conveying any rights or permission to manufacture, use, or sell any patented invention that may in any way be related thereto.

The information furnished herewith is made available for study upon the understanding that the Government's proprietary interests in and relating thereto shall not be impaired. It is desired that the Judge Advocate (WCJ), Wright Air Development Center, Wright-Patterson Air Force Base, Ohio, be promptly notified of any apparent conflict between the Government's proprietary interests and those of others.



WADC TECHNICAL REPORT 52-227

**PROPERTIES OF TEMPERATURE-RESISTANT MATERIALS
UNDER TENSILE AND COMPRESSIVE FATIGUE STRESS**

*B. J. Lazan
E. Westberg*

Syracuse University

November 1952

*Materials Laboratory
Contract No. AF 33(038)-18903
RDO No. 614-16*

Wright Air Development Center
Air Research and Development Command
United States Air Force
Wright-Patterson Air Force Base, Ohio

FOREWORD

This report was prepared by Syracuse University, B. J. Lazan* and E. Westberg, under Contract No. AF 33(038)-18903 with Wright Air Development Center, Wright-Patterson Air Force Base, Ohio, identified by Research and Development Order No. 614-16, "Fatigue Properties of Aircraft Structural Materials". It was administered under the direction of the Materials Laboratory, Directorate of Research, Wright Air Development Center, with Mr. W. J. Trapp acting as project engineer.

*Professor of Materials Engineering, University of Minnesota, Minneapolis, Minn., formerly at Syracuse University.

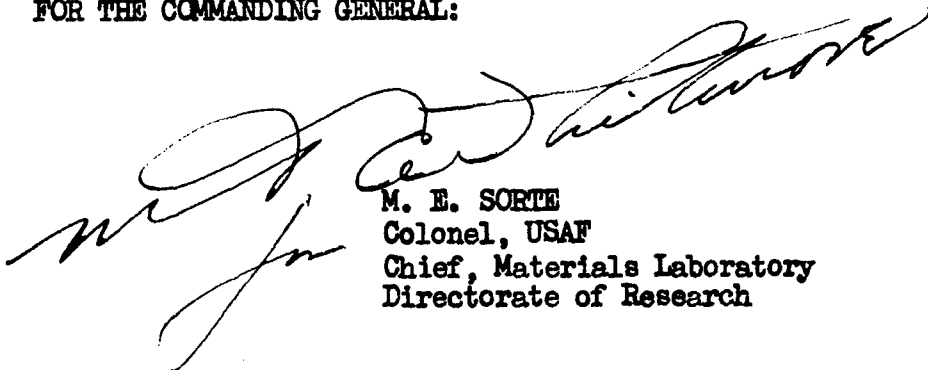
ABSTRACT

Newly developed grips and machine improvements are described for fatigue loading under direct stress (tension-compression) ratios of alternating to mean stress from zero to infinity. Data are presented to indicate the uniformity of stress distribution possible with these grips and accuracy of the average stress. Dynamic creep, rupture and ductility data are reported on N-155, S-590 and Vitallium at 1350° and 1500° F. under direct stress combinations from static to reversed loading. Stress range diagrams (alternating stress versus mean stress) are presented to indicate the stress combination which will produce rupture and various degrees of creep in 5 to 1500 hours. Per cent elongation data are analyzed in terms of alternating-to-mean stress ratio and stress magnitude, and it is shown that both are significant variables. Elongation up to the start of third stage of creep is also analyzed in terms of stress ratio and stress magnitude and only stress magnitude was found to be significant. The implications of these findings are discussed.

PUBLICATION REVIEW

This report has been reviewed and is approved.

FOR THE COMMANDING GENERAL:



M. E. SORTE
Colonel, USAF
Chief, Materials Laboratory
Directorate of Research

TABLE OF CONTENTS

	<u>Page</u>
I. Introduction	1
II. Testing Equipment	1
III. Stress Distribution Studies and Calibration	4
IV. Design and Preparation of Test Specimens	7
V. Test Materials	8
VI. Test Data and Discussion	8
VII. Summary and Conclusions	17
Bibliography	40
<u>LIST OF TABLES</u>	
Table 1. Test Data for N-155 (NA) at 1500°F.	19
2. Test Data for N-155 (NA) at 1350°F.	20
3. Test Data for Vitallium Alloy at 1500°F. and 1350°F.	21
4. Test Data for S-590 Alloy at 1500°F. and 1350°F.	22
<u>LIST OF ILLUSTRATIONS</u>	
Fig. 1. Photograph of Dynamic Creep and Rupture Machine	23
2. Grip-Specimen Assembly in Reversed Stress Fatigue Testing	23
3. Schematic Diagram of Vibration Locking Attachment	24
4. Calibration Specimen for Stress Distribution Tests	25
5. Stress Distribution in Test Section of Specimen Held by Early Version of Tension Compression Grip	25
6. Drawings of Dynamic Creep and Rupture Specimens Type A and B	26
7. Total Creep Versus Time Curves at Various Stresses and Stress Ratios for N-155 at 1350°F.	27
8. Total Creep Versus Time Curves at Various Stresses and Stress Ratios for N-155 at 1500°F.	28
9. Time to Rupture, 0.5% and 2% Creep Versus Mean Stress During the Stress Cycle for N-155 at 1350°F. and 1500°F.	29
10. Time to Rupture, 0.5% and 2% Creep Versus Maximum Stress During the Stress Cycle for N-155 at 1350°F. and 1500°F.	30
11. Static and Dynamic Stress Combinations Which Cause Rupture, 2% and 0.5% Creep in Hours Indicated for N-155 at 1500°F. and 1350°F.	31
12. Effect of Dynamic Stress Ratio A and Stress Magnitude on Percent Elongation of Alloy N-155 at 1350 and 1500°F.	32
13. Effect of Dynamic Stress Ratio on Elongation at Failure in 150 Hours for Alloy N-155 at 1350 and 1500°F.	33
14. Effect of Dynamic Stress Ratio and Mean Stress on % Creep up to Third Stage on Type A Specimen N-155.	34
15. Time to Rupture, 0.5% and 2% Creep at 1350°F. and 1500°F. Under Static and Dynamic Tensile Stress for S-590	35
16. Static and Dynamic Stress Combinations Which Cause Rupture, 2% and 0.5% Creep in Hours indicated For S-590 at 1500°F. and 1350°F.	36
17. Effect of Dynamic Stress Ratio and Mean Stress on Percent Elongation of Type A Specimens S-590.	37
18. Time to Rupture, 0.5% and 2% Creep at 1350°F. and 1500°F. Under Static and Dynamic Tensile Stress for Vitallium.	38
19. Static and Dynamic Stress Combinations Which Cause Rupture, 2% and 0.5% Creep in Hours Indicated For Vitallium at 1350°F. and 1500°F.	39

I. INTRODUCTION

Present day developments in new and improved devices operating at increasingly higher temperature have imposed challenging problems on both the metallurgist and machine designer. One of these problems is the evaluation and interpretation of the mechanical properties of materials at elevated temperatures, particularly under cyclic stress. As more data on service failures of parts exposed to elevated temperatures are accumulated and analyses undertaken (1), the increasing importance of cyclic stress as a cause for service failure becomes apparent.

The work reported in this paper represents a continuation and extension of earlier research (2) by one of the authors on the effect of various combinations of static and alternating direct stress on the creep, rupture, elongation and other properties of temperature-resistant materials at high temperature. In the earlier work, fatigue stress in the tension only was investigated, whereas in this program the stress ratios A^* in the range from zero (static test) to infinity (reversed stress fatigue test) are studied.

Prior work in the field of dynamic creep and rupture of materials at elevated temperature is reviewed in reference (2). Current work in this field is described in reference (3).

*Stress Ratio A is the ratio of the alternating stress component to the mean stress (static or preload component) during the stress cycle (see reference (2)).

II. TESTING EQUIPMENT

The testing machines and measuring equipment used in this program are the same as described in reference (2) except for the improvements and additions described below. Alternating force is imposed by a special centrifugal force type oscillator and static preload is applied by calibrated springs and maintained constant by an automatic follow up system. Creep is measured with a special micrometer microscope assembly which utilizes stroboscopic light to

"fix" for measuring purposes the platinum targets attached to the test specimens. A photograph of this dynamic creep and rupture machine with the furnace, creep measuring microscopes and an extra tension-compression fatigue grip is shown in Fig. 1.

Several changes were made in the original machine described in reference (2) in order to increase its capacity from ± 1000 lbs alternating force to ± 5000 lbs capacity so that fatigue testing under reversed stress would be possible without reducing the size of the test specimens used in the earlier work (2). The machine is now designed so that alternating force cages are available for ± 1000 lbs, ± 2000 lbs, and ± 5000 lbs capacity, and the preload springs are available for 1000, 5000, and 10,000 lb capacity. Since these parts may be used interchangeably and in various combinations, the advantages of a multi-range machine are realized in that medium capacity tests may be performed and yet accuracy is retained at low capacity.

The original machine was used for fatigue testing in the tension range only and therefore utilized simple spherical head type of grips. It was therefore necessary to develop a new set of grips, described below, for fatigue testing in both the tension and compression range.

A schematic diagram of the reversed stress grips is shown in Fig. 2. The upper stationary platen R is the same as shown in Fig. 1 and B is the reciprocating platen attached to the centrifugal force cage E. Two nuts, K and L, threaded on each end of test specimen S, are clamped between outer tubes (A for the upper grip and D for the lower grip) and inner tubes G. The clamping force is exerted by screws C which apply the load through the Belleville springs H. The functions of springs H is to maintain reasonable constant preload force in the gripping nuts at all times, even under differential expansion and other influences which may tend to affect tightness. The upper tube A is rigidly attached to the upper crosshead R being locked in place between three screws Y at 120° spacing and three cap screws Z at

120° spacing but offset from screws Y by 60°. The lower outer tube D is attached to the reciprocating part B by a threaded ring F, which is removeable in order to keep the lower end of the specimen grip assembly smaller than the inside diameter of the furnace for ease in setting up the test. All grip parts are made rigid to minimize stress non-uniformity in the test specimen, and yet have relatively small cross-sectional area so as to minimize heat transfer from the furnace M, which surrounds the specimen and inner parts of the grips, to the remaining parts of the machine.

One advantage of this type of grip is that the specimen can be held through relatively simple threaded ends requiring only standard fits and tolerances. Furthermore, the threaded end of the specimen and the holding nuts K and L can be adequately preloaded by screws C so as to avoid excessive motion, and resultant fretting and fretting corrosion in the threads and at the joints. "Freezing" of the thread is therefore reduced and removal of the nuts from the specimen even after prolonged fatigue tests is usually accomplished with reasonable ease. Furthermore, should the nuts strongly adhere to the specimen threads, or should they gradually deteriorate during prolonged use, only the relatively minor parts of the grips (the nuts) are involved and the major parts of the grips are not affected.

The procedure used in setting up and aligning the specimen arm assembly in the machine is as follows. The grip parts and specimen, assembled on a bench, are placed in horizontal centers so that the run-out of the grip-specimen assembly may be determined. Screws C and adjusting screws W may then be preferentially tightened to reduce the run-out as much as possible, always to within a few thousandths of an inch. The assembly is then inserted downward through the furnace, ring F is threaded onto the lower end of D, and the whole assembly is rigidly locked to the lower head with the screws shown (top end free). After the specimen, grip assembly, and attached parts attain the testing temperature and stabilize (the upper end of the grip assembly being

allowed to expand freely during this period) set-screws Y are carefully made to contact the lower surface of the flange at the top of A. An electrical contactor is used for this operation to avoid imposing undesired initial stress in the specimen. After the three set screws Y have been accurately located (the purpose of the spring at the bottom of these set-screws is to reduce the backlash and facilitate accurate adjustment) cap screws Z are tightened rigidly locking the flange to the upper cross head R. A torque wrench is used for this operation since unequal tightening may induce bending stress. The set-up is now ready for the test.

A special attachment shown as part C in Fig. 1 was developed for locking the vibrating system after the specimen breaks. This is particularly desirable for fatigue tests which enter the compression range so that the fractured portions of the test specimen remain unbattered for subsequent fracture and metallurgical examinations. The operation of this vibration locking attachment may be understood by referring to Fig. 3. T is the top of the testing machine and R is the reciprocating platen of the oscillator cage. Part F which is attached to R contains an actuator for trigger D and a locking hole which is engaged by bolt C. The trigger D and bolt C are attached and guided by block B, which is bolted to table top T. The operating sequence of this device is as follows: after the specimen breaks, the amplitude of vibration increases and part F actuates trigger D which releases bolt C which is driven by spring E to engage lock F. The vibration locking attachment effectively restricts the vibrations and the fractured surfaces of the specimens are retained in good condition. Fracture and metallographic studies undertaken as part of this program are discussed in reference (4).

III. STRESS DISTRIBUTION STUDIES AND CALIBRATION

The production and maintenance of a uniform stress distribution in direct stress fatigue specimens constitutes a most important work. Very small errors in alignment in the specimen-grip assembly, such as setting of the screws Y 0.001" too high, for example, may result in very serious extraneous bending stress.

Needless to say, the presence of extraneous bending stress may seriously affect the reliability of the test data. As a result of these observations particular emphasis was placed in this work on procuring and maintaining uniform stress distribution in the test specimen.

The production of consistent and significant direct-stress fatigue data requires that bending stress be avoided during the following operations:

- (a) Clamping of specimen-grip assembly in fatigue machine
- (b) Application of preload
- (c) Application of alternating force.

The presence and magnitude of these types of undesired bending were determined by direct measurement of strain on the test section as described below.

Special calibration specimens were made identical in test section to type A specimens in Fig. 7 and six SR-4 wire resistance gages were attached to it as shown in Fig. 4. Three gages, L_t , M_t , and R_t were attached at the upper portion of the specimen test length at 120° angle as shown, and three were attached to the lower portion of the test section. Electrical connections were made so that gages could be read independently or combined to give average effects. This set-up permits measurement of not only average stress but also stress distribution on both the top and bottom cross-section of the specimen. The calibration specimen and grip assembly is shown on the left side of the testing machine pictured in Fig. 1.

A similar calibration specimen, except with only one set of three gages at the test section, was also made to study stress distributions in the single fillet specimen type B in Fig. 6.

The output of the SR-4 gages during clamping static preload increase and application of alternating force was measured by an Ellis BA-11 strain analyzer used in conjunction with an oscilloscope. Brush AC-DC analyzer recordings were also used, particularly in studying clamping stress. The oscilloscope was also used to study wave form of the cyclic stress.

The early unrefined version of the tension-compression grip was found to produce considerable non-uniformity in stress distribution during clamping as well as during the application of alternating stress. Figure 5 shows this stress non-uniformity during one calibration test on one of the first grip set-ups; the alternating stress distribution across and along the test section varied as much as 25%. In this figure the alternating stress setting of the machine, or the alternating stress desired in the specimen, is shown along the right ordinate. The actual stresses existing at various points around the periphery of the test sections are shown by the experimental points in this figure. The gage location $L_T, M_T,$ and R_T , refer to the left, middle, and right gage respectively at the top of the test section as shown in Fig. 4, whereas $L_B,$ and $M_B,$ and R_B refer to the gages at the bottom of the test section. Since these gages are 120° apart, and since a cross-sectional plan remains a plane, the curve shown joining the three points is a sine wave. The implication of such large variations in stress distribution is apparent, the stress at some points in the specimen being as much as 25% higher than desired.

Similar studies were made on clamping stress, which was found to be seriously large in unrefined grips.

As a result of stress distribution measurements of the type discussed above and harmonic indications by the cathode ray oscilloscope, several corrective steps were taken to improve the grips. This led to the present grip design and setting-up procedure described previously, in which the clamping stress and the non-uniformity stress distribution across the test section is generally within 4%. Considerable calibration data were procured with refined grips, but these are not shown in this condensed report.

Careful calibration was also undertaken of alternating force produced by the machine, three different methods of analyses being used. Calibration data determined by all three methods (two experimental and one theoretical)

fell within a $\pm 3\%$ scatter band, which accuracy is considered entirely adequate for fatigue work. Description of these calibration methods is outside the scope of this paper.

IV. DESIGN AND PREPARATION OF TEST SPECIMENS

The two different types of test specimens shown in Fig. 6 were used in this project, the test section being 1/4 inch diameter in both cases. In general, test specimen type A was used for stress ratios A of 0, 0.25, and 0.67 and type B specimen for ratios of 2.0 and infinity.

The straight sectioned type A specimen was used for the lower stress ratios so that not only rupture and fatigue properties could be determined, but also to enable measurement of dynamic creep. The single fillet type B specimen was used at the higher stress ratios because:

- (a) At high stress ratios dynamic creep becomes less important than rupture and fatigue properties (2) and is not measured. Therefore, the simpler single-fillet specimen type B is adequate.
- (b) Under reversed stress the bending and buckling effects are likely to be less serious in the stiffer type B specimen.
- (c) At high levels of alternating stress the hysteresis damping (5) in the materials may internally heat the specimen seriously. Other factors being equal the larger the volume of metal at stress the greater the internal heating. Consequently, specimen type B, with its small test volume is less likely to be troublesome due to internal heating. However, even in the type B specimen enough internal heat was generated due to hysteresis damping to increase the temperature of the specimen 150°F in some tests.
- (d) Type B specimens are easier to make than type A specimens.

A few check tests at $A = 0.67$ indicated that rupture data procured on the type B specimens are in agreement with data on type A specimens.

All specimens were longitudinally polished using an abrasive belt method. Specimens of Vitallium and S-590 were machined and finished in a specially developed contour block belt polisher as explained in reference (2) and N-155 specimens were prepared by a somewhat similar method by the University of Michigan as explained in reference (3).

V. TEST MATERIALS

Date on the following three test materials are reported in this paper:

- (a) S-590, Allegheny Ludlum Heat 42198, water quenched from 2250°F, aged at 1400°F for 16 hours, and furnace cooled.
- (b) Vitallium, Haynes Stellite Heat 573, precision cast, aged at 1350°F for 50 hours and furnace cooled.
- (c) N-155, Universal Cyclops Heat A-1726, water quenched from 2200°F, aged at 1400°F for 16 hours, and air cooled.

Additional metallurgical details and photomicrographs are given in reference (2) for the first two materials and in reference (3) for N-155.

VI. TEST DATA AND DISCUSSION

The primary type of dynamic creep, rupture, and ductility data procured for each of the three materials are indicated in Tables 1 to 4 and Fig. 7 and 8. The behavior of N-155 shall be discussed first.

Referring to Table 1 for N-155 at 1350°F, a series of approximately seven tests were performed at each of five stress ratios A at stress levels to cause failure in from approximately 1 to 5000 hours. Table 1 shows the mean, alternating, crest (or maximum), and trough (or minimum) stress (see Fig. 1 of reference (2) for more complete definition of terms) maintained constant during the life of the specimen. At high stress ratios ($A = 1.64$ and ∞) fatigue or rupture time and ductility are of primary importance and dynamic creep became relatively unimportant (2). Therefore dynamic creep data were not procured at these high stress ratios. At the lower stress ratios ($A = 0.67, 0.25$ and 0) the rupture time and ductility are still of primary importance in many applications, but in others static and dynamic creep may govern the design.

Consequently at these lower stress ratios the dynamic creep was measured during the progress of the test (see reference (2) for description of methods of measurement) and plotted as shown in Fig. 7.

The elongation data listed in Table 1 and subsequent tables are given as both the uncorrected values and the corrected values. The uncorrected percent elongation was determined in the usual way from measurements of the length of the broken specimens matched at the fractured section. The corrected

percent elongation was determined by subtracting from the length measured above the length of the maximum surface opening at the properly matched fractured section. This surface opening correction is intended to eliminate purely localized deformation which occurs during the final separation at the fracture. At low stress ratios this correction is generally very small whereas at high stress ratios it is generally quite significant.

The equivalent test section length of the specimen type A shown in Fig. 6 was calculated to be two inches as explained in reference (1). The equivalent percent elongation listed in Table 1 for type B specimens, which has no straight test section, was determined by multiplying the corrected inches elongation of these specimens by a constant. This constant was determined experimentally from elongation data procured under identical conditions on both type A and B specimens (compare specimens JT-11 with JL-8 and JD-5 with JI-14). It is recognized that this method of determining the percent elongation from inches elongation of the type B specimen is approximate since the "constant" relating the two is probably somewhat dependent on stress magnitude and stress ratio (since creep is probably not expressible as a function of stress to some fixed exponent n). However, it is believed that this approach is sufficiently accurate to reveal the significant ductility trends discussed later.

Each of the static and dynamic creep curves shown in Fig. 7 is based on approximately 25 experimental points, now shown for clarity, which generally had very small scatter. The final reading taken prior to rupture is shown by the symbol (R), which of course may be considerably less than the total elongation since in many cases this reading preceded fracture by hours. The creep data shown in Fig. 7 are plotted within log-log coordinates to enable including the creep-time relationship up to failure and yet not condense the first part of the curve beyond recognition and use. Being a log-log plot, the customary three stages of creep are not of course recognizable.

The log-log plot of creep versus time for N-155 at 1500°F is shown in Fig. 8.

Referring to Figs. 7 and 8 it may be observed that at 1350°F the higher stress ratios generally produce a flatter creep versus log time curve, but otherwise the shapes of the curves for equal life are quite similar. At 1500°F the increasing stress ratio does not appear to significantly affect slope of the log-log curves. Other observations apparent from Fig. 7 and 8 regarding the effects of stress ratio and stress magnitude will be more apparent from derived and reduced curves discussed below.

In order to reveal more clearly the trends in creep and rupture behavior with temperature, stress, and stress ratio, the data obtainable from Fig. 7 and 8 are replotted in Fig. 9 on a mean stress basis. These curves show the hours for rupture, and hours for 2% and 0.5% creep for various stress ratios A as a function of mean stress. Also shown along the abscissa besides the time scale are numbers of stress cycles (machine operates at 3600 rpm). These diagrams include the data on type A specimen at stress ratios of 0, 0.25, and 0.67 and the fatigue strength of type B specimens at the stress ratio of 2. Reversed stress fatigue data (mean stress equals zero) cannot of course be shown in this diagram. Dynamic creep data were not procured on the type B specimens since the creep properties become relatively less important than the rupture properties at the high stress ratios (2). Furthermore, the single fillet type B specimen are not suitable for quantitative creep measurements because of the indeterminate gage length. They are suitable however for comparative elongation studies as discussed previously.

A significant observation apparent from Fig. 9 is smaller (semi-logarithmic) slope of the large stress ratio curves ($A = 0.67$ and 2) compared to those for small stress ratio ($A = 0$ and 0.25). This difference in slope, which is larger at 1500°F than at 1350°F, means that even though the allowable mean stress for short life is considerably smaller at high stress ratios than

at low stress ratios, the allowable mean stress for long life (say in the region of 2000 hours) is quite independent of stress ratio in the range from 0 to 1.64. The same observations may be made regarding creep. These observations will be discussed further in connection with the stress range diagrams presented later.

In order to present still another viewpoint and also to permit the inclusion of reversed stress data, the rupture and creep properties are shown in Fig. 10 as a function of maximum or crest stress during the vibration cycle. This figure includes data for both the type A and type B specimens, and where both specimens were tested at the same stress ratio of $A = 0.67$ the strength data are in reasonably good agreement. Here again the high stress ratio curves have smaller slope than those at low stress ratios, the curves at $A = \infty$ being practically horizontal. Considering maximum stress as a criterion, the allowable stress for long life increases with increasing stress ratio. The same is true for short life for the stress ratios of 0, 0.25, and 0.67. However, the allowable maximum stress for short life at $A = 1.64$ and $A = \infty$ is substantially less than for the smaller stress ratios.

In general the slope trends discussed above are associable with the primary cause of failure. At small stress ratios where creep and stress rupture effects predominate the slopes of these curves are rather large, but at high stress ratios which fatigue becoming important the slopes are rather flat. It should also be mentioned that the curves shown in Fig. 10 for the high stress ratios of $A = 1.64$ and infinity are the usually S-N fatigue curves except that they do not display the usually S-N knee. Therefore, a fatigue limit does not appear to exist under these conditions.

Of the various types of diagrams presented to show rupture and creep data the stress range diagrams shown in Fig. 11 are probably the most concise and revealing. These diagrams show the combinations of static preload and alternating stress at 1350° and 1500° F which result in rupture and 2% and 0.5%

creep in 5, 15, 50, 150, 500, and 1500 hours. The number of stress cycles imposed during the dynamic test for each of these lives are 1.07, 3.22, 10.7, 32.2, 107, and 322 millions of cycles, respectively. As mentioned previously dynamic creep data were procured over the stress ratio from $A = 0$ to 0.67, whereas rupture data were obtained over the range from $A = 0$ (horizontal line) to $A = \infty$ (vertical line).

Referring to the stress range diagrams for rupture and creep of N-155 at 1350° and 1500° F the following observations may be made:

- (a) In general, small amplitudes of alternating stress, say up to 35% of the mean stress, do not greatly affect the life or creep associated with the same mean stress applied statically. In fact, the addition of small alternating force to a mean stress may even increase slightly the life at the corresponding mean stress. These observations are more apparent at long lives as compared to short lives and at 1500° F as compared to 1350° F.
- (b) Since the distance between curves representing different hours of life indicates the effect of time (or number of stress cycles), the lower the stress ratio the greater the effect of time on strength. Therefore, creep and rupture are much more time-dependent than fatigue.
- (c) The ratio of reversed stress fatigue strength to static rupture strength is greater at 1500° F than at 1350° F, averaging approximately 1.4 compared to 1.26 for the range of lives investigated.
- (d) The stress range diagrams for both rupture and creep fit a circular or Gerber's (6) relationship more closely than the straight line or modified Goodman relationship. Therefore design on the basis of the latter two relationship will be on the conservative side.

A property frequently used by the designer to indicate the ductility of a material is the percent elongation. Curves showing percent elongation at 1350° F and 1500° F as a function of mean stress and stress ratios from 0 to 0.67 for type A specimens and from 0.67 to ∞ for type B specimens are given in Fig. 12. Although there is considerable scatter in this data, in general it may be concluded that for most cases the higher the stress ratio the smaller is the percent elongation. At 1500° F the mean stress is also an important variable in determining percent elongation; the lower the stress and the longer the life, the smaller is the percent elongation. However, this stress magnitude effect decreases with increasing stress ratio; under static conditions ($A = 0$) the percent elongation may increase more than three times with increasing stress level, whereas under partially reversed stress ($A = 1.64$) the

percent elongation is practically independent of stress level. At 1350°F however, stress level is quite insignificant in determining percent elongation; stress ratio is the most significant variable.

Figure 13 is an attempt to show the effect of stress ratio on percent elongation. Since stress level, or life, may be a variable under certain conditions, the data plotted in Fig. 13 is based on a life of 150 hours. Of course, similar diagrams for other lives can also be made from the available data.

Under reversed stress conditions, one would expect insignificant elongation. The data show this to be reasonably true at 1350°F, but at 1500°F approximately 2.5% elongation was measured. This may be due either to the difference in tension and compression creep properties or the inaccuracy of the gap subtraction method used to determine corrected elongation.

Although the elongation data diagrammed in Fig. 12 are "corrected" values, in that they exclude the largest surface gap at the fracture as explained previously, they still include the effects localized necking which precedes fracture. In some respects the elongation data might be more significant if such localized necking effects could be excluded. This can be done by considering the elongation during the first two stages of creep only, and excluding the third stage during which the localized necking effects occur.

In order to procure elongation up to the third stage of creep, the semilogarithmic creep versus time data shown in Figs. 7 and 8 were replotted on a linear basis. For brevity, these figures are not included in this paper. An attempt was then made to determine the creep up through the second stage, up to the start of the third stage, where the creep-time curves cease to be linear and where necking generally commences. However, the end of the second stage of creep and the beginning of the third or final stage is something

not well defined. Therefore, in order to define this point more accurately the following approach was used.

The second stage of creep was considered to end at the point where the minimum slope (second stage creep) line intersects a tangent to the third stage creep line at a point having 50% greater slope than the second stage creep line.

Although this approach is arbitrary, it did uniquely define a transition point and in cases having a distinct beginning to third stage creep insignificant error was observed.

The elongation through the first two stages of creep, determined as explained above, are diagrammed in Fig. 14 as function of mean stress and stress ratio. Referring to this figure there appears to be three distinguishable zones:

- (a) At low mean stresses there is relatively little elongation and scatter, and stress ratio effects are not distinguishable.
- (b) At high stress levels considerably higher elongation occurs and scatter increases pronouncedly without revealing any apparent stress ratio effects.
- (c) The transition zone between these two regions displays a rather abrupt increase in elongation.

In none of the three zones is there any evidence of stress ratio effects similar to those displayed in the total elongation diagrams. It appears therefore, that the major effects of stress ratio on total elongation occur during the third stage of creep, at least for N-155 at stress ratios ranging from 0 to 0.67.

The two stage elongation data plotted in Fig. 14 shows similar patterns and order of magnitudes for both 1350° and 1500°F. The only significant difference apparent is the stresses at which the transition zone discussed above occurs.

The significance of three zones observed in the two-stage elongation data is not yet clear. It has not been possible as yet to associate this elongation behavior with fracture characteristics (4). Other materials discussed below do not reveal such a pattern

A discussion of whether or not the two-stage creep data is better than total percent elongation in indicating the "true ductility" of a material is beyond the scope of this paper.

During the reversed stress fatigue testing of N-155 at 1350°F several interesting observations were made relating to the damping energy (5) in the material and the resultant rapid increase in specimen temperature immediately after the start of the alternating stress. At $\pm 36,000$ psi this increase was 25°F, at $\pm 38,000$ psi it was 120°F, and at $\pm 40,000$ psi it was 150°F, all these temperature increases generally occurring within a minute after starting the alternating load. No significant temperature increases were observable under like conditions at 1500°F. During 1000°F and room temperature tests, not reported in this paper, temperature increases as large as 400°F and 1200°F, respectively, were observed during the start of the test.

These temperature increases of course affect testing techniques as related to presetting the furnace at a temperature lower than desired to allow for the increase caused by alternating force. However, more significant is the implication of these increases in terms of internal hysteresis damping. The temperature increases are caused by internal hysteresis damping of the material, and therefore provide a rough measure of damping energy. The higher damping at 1350°F as compared to 1500°F, as indicated by these temperature increases, are now being quantitatively determined in this rotating beam test described in reference (5). In this connection, attention is directed to damping data given in reference (5) on S-816 at room temperature, 900°F and 1600°F. The peak values at 900°F indicate the possibility that N-155 may display reducing damping capacity with increasing temperatures beyond a certain limit.

Dynamic creep and rupture data similar to that present above for N-155 were also procured on S-590 and Vitallium at stress ratios A of 0, 0.25, and 0.67 and temperatures of 1350°F and 1500°F. However, for brevity only rupture

and creep versus time diagrams (Figs. 15 and 18), the stress range diagrams (Figs. 16 and 19) and the ductility curves for S-590 only (Fig. 17) are presented. Although much of those data were included in reference (2) there are sufficient new data to justify including of the extended curves for these materials in this paper. The stress range diagram for 2% creep for Vitallium does not include the region at $A = 0.67$ since most of the Vitallium specimens failed before attaining this elongation (2).

The general patterns revealed in Fig. 11 for N-155 and discussed above are also apparent in the stress range diagrams of Figs. 16 and 19. No attempt is made in this paper to undertake a comparative evaluation of these materials since properties other than those considered here, such as corrosion resistance, thermal shock behavior, fabrication properties, etc. must be considered. However, it might be stated that Vitallium does display the best dynamic creep and rupture resistance at low stress ratios and for short lives. However, time at load affects Vitallium more pronouncedly than the other two materials (compare slopes in Figs. 9, 15, and 18 or compare distance between curves for different lives in Figs. 11, 16, and 19), so that this superiority does not hold up for long life.

The percent elongation curves shown in Fig. 17 for S-590 are somewhat different in character than those shown for N-155 in Figs. 12 and 14. The separation and change in slope according to stress ratio A is not nearly as distinct at 1500°F for S-590 as for N-155. Furthermore, the creep to third stage does not display a transition zone in S-590 as was observed in N-155. However, the N-155 pattern is partially followed in that the creep to third stage does fall approximately on the same line for all stress ratios and increases with increasing stress magnitude. Although the elongation diagrams for Vitallium are not included in this paper the same general observations can be made; the separation of total elongation according to stress ratio is even less distinct and the creep to third stage is quite independent of stress

magnitude and stress ratio in the range investigated.

VII. SUMMARY AND CONCLUSIONS

Fatigue, dynamic creep, rupture, and elongation data, procured with newly developed direct stress fixtures, are presented for N-155, Vitallium and S-590 at 1350° and 1500°F.

The dynamic properties of N-155 were procured at alternating-to-mean stress ratios ranging from zero (static stress) to infinity (reversed stress fatigue) and the following observations were made:

- (a) At high stress ratios (fatigue range) there is a relatively small decrease in strength with time or with number of cycles, whereas at low stress ratios (creep and stress rupture range) the strength is highly dependent on time. Thus, although the reversed stress fatigue strength is generally lower than the static rupture strength for relatively short lives, the opposite is generally true for long duration tests.
- (b) In general small amplitudes of alternating stress, say up to 35% of the mean stress, do not affect life or creep associated with the same mean stress applied statically. In fact, the addition of small alternating stress to a mean stress may even increase slightly the life and decrease the creep at the corresponding mean stress. These observations are more apparent at long lives as compared to short lives and at 1500°F as compared to 1350°F.
- (c) The stress range diagrams for both fatigue and stress rupture and also for creep fit a circular or Gerber's relationship more closely than the straight line or modified Goodman law.

Vitallium and S-590 alloy, investigated in the stress ratio range from 0 to 0.67 displayed general behavior patterns similar to discussed above N-155.

In general, the total elongation to fracture decreases with increasing stress ratios, being practically zero under reversed stress. Although there is considerable scatter in total elongation data, this elongation increases with mean stress in all cases except N-155 and Vitallium at 1350°F.

In order to eliminate the confusing effects of localized necking during third stage creep and to procure perhaps a better measure of "true ductility," the elongation during the first two stages of creep was determined and diagrammed as a function of mean stress and stress ratio in the range from 0 to 0.67. In general there is less scatter in this type of elongation than in total elongation. Furthermore stress ratio appears to have little

influence and data for all stress ratios fall on the same curve. It appears therefore, that the major effects of stress ratio on total elongation occur during the third stage of creep, at least in the range of stress ratios from 0 to 0.67.

Although the two-stage elongation increases gradually with stress magnitude from S-590 and 1350°F and 1500°F and Vitallium at 1500°F, it is reasonably constant at all stress for Vitallium at 1350°F. In the case of N-155 at both 1350°F and 1500°F, as stress magnitude is increased there is a uniform and gradual increase in two-stage elongation with very little scatter followed by a transition zone of rapid increase, and at high stress a relatively large but reasonably constant elongation is displayed. Relatively large scatter in two-stage elongation occurs in this high stress region.

TABLE 1; TEST DATA FOR N-155 (NA) at 1500° F.

Specimen Number	Stress Ratio A	Applied Stress-KSI				Hours to Rupture	% Elongation	
		Mean	Alter.	Crest	Trough		Uncor-rected	Cor-rected
JP-12	0	7.0	0	7.0	7.0	5.9*		
JI-5	0	11.0	0	11.0	11.0	1004.6	11.6	.9.1
JE-5	0	13.0	0	13.0	13.0	398.5	11.7	11.3
JH-10	0	15.0	0	15.0	15.0	221.2*	17.0*	16.6*
JV-8	0	17.5	0	17.5	17.5	67.2	25.2	24.3
JA-16	0	19.0	0	19.0	19.0	47.9	28.0	27.4
JO-6	0	20.0	0	20.0	20.0	24.9	34.4	34.1
JB-5	0	22.5	0	22.5	22.5	20.7	36.4	36.2
JR-10	0.25	8.8	2.2	11.0	6.6	4117.0	11.1	11.0
JH-5	0.25	10.0	2.5	12.5	7.5	2790.1	11.9	11.3
JF-5	0.25	14.0	3.5	17.5	10.5	410.9	15.4	14.8
JT-5	0.25	15.2	3.8	19.0	11.4	382.3*	9.6*	9.3*
JE-12	0.25	16.8	4.2	21.0	12.6	209.5	21.3	21.1
JL-5	0.25	19.2	4.8	24.0	14.4	83.4	19.9	19.6
JM-21	0.25	22.0	5.5	27.5	16.5	14.9	30.0	29.7
JW-4	0.25	24.0	6.0	30.0	18.0	8.0	28.1	27.6
JS-5	0.67	8.0	5.3	13.3	2.7	4066.0	5.9	5.5
JT-11	0.67	12.0	8.0	20.0	4.0	640.0	10.2	9.6
JW-6	0.67	15.0	10.0	25.0	5.0	226.5	15.8	15.2
JD-5	0.67	16.8	11.2	28.0	5.6	85.1	18.3	17.6
JL-10	0.67	18.6	12.4	31.0	6.2	36.3	21.8	21.1
JG-12	0.67	21.0	14.0	35.0	7.0	19.7	13.7	13.0
JV-13	0.67	22.2	14.8	37.0	7.4	10.9	19.9	18.5
All specimens above are type A								
All specimens below are type B								
							Corrected Elong.	
							Inches	Equiv. %
JL-8	0.67	12.0	8.0	20.0	4.0	837.5	.057	11.4
JI-14	0.67	16.8	11.2	28.0	5.6	125.1	.084	16.8
JY-9	1.64	9.0	14.8	23.8	5.8	1273.0		
JK-11	1.64	11.0	18.0	29.0	7.0	343.7	.025	5.0
JY-10	1.64	12.0	19.7	31.7	7.7	150.0	.037	7.0
JS-13	1.64	13.0	21.3	33.3	8.3	50.7	.039	8.0
JW-9	1.64	14.0	23.0	37.0	9.0	14.7	.032	6.5
JR-14	1.64	15.0	24.6	39.6	9.6	0.4	.029	6.0
JX-9	∞	.0	21.8	21.8	21.8	1048.0	.014	2.8
JU-14	∞	0	24.3	24.3	24.3	536.1		
JI-15	∞	0	24.6	24.6	24.6	106.1	.017	3.4
JH-15**	∞	0	25.3	25.3	25.3	106.9	.012	2.4
JS-14	∞	0	25.3	25.3	25.3	8.3	.008	1.6

* Thermocouple or other difficulties caused overloading or overheating of specimen at time indicated, or specimens stopped before failure.

** Statically loaded for 100 hours at 14,000 Psi prior to dynamic loading.

TABLE 2: TEST DATA FOR N-155 (NA) at 1350° F.

Specimen Number	Stress Ratio A	Applied Stress-KSI				Hours to Rupture	% Elongation	
		Mean	Alter.	Crest	Trough		Uncor-rected	Cor-rected
JZ-16	0	17.5	0.0	17.5	17.5	3185.0	15	14
JC-5	0	22.0	0.0	22.0	22.0	1114.0	17	17
JA-20	0	25.0	0.0	25.0	25.0	208.0	28	28
JM-22	0	30.0	0.0	30.0	30.0	58.3	24	21
JY-6	0	35.0	0.0	35.0	35.0	22.8	31	30
JJ-6	0	40.0	0.0	40.0	40.0	4.0	18	17
JQ-5	0.25	17.5	4.4	21.9	13.1	3783.0	14	14
JU-13	0.25	19.0	4.7	23.7	14.2	2683.0	25	25
JG-5	0.25	23.2	5.8	29.0	17.4	682.0	22	21
JF-11	0.25	25.0	6.2	31.2	18.7	518.0	20	20
JC-10	0.25	27.5	6.8	34.3	20.7	165.0	24	23
JK-13	0.25	30.0	7.5	37.5	22.5	52.2	19	19
JB-13	0.25	33.0	8.2	41.2	24.7	27.2	17	17
JN-6	0.25	37.0	9.2	46.2	27.8	7.6	18	18
JQ-14	0.67	17.5	11.7	29.2	5.8	3349.0	8	7
JX-6	0.67	17.5	11.7	29.2	5.8	2821.0	11	11
JD-13	0.67	18.0	12.0	30.0	6.0	2500approx		
JI-12	0.67	19.0	12.6	31.6	6.3	2107.0	12	11
JA-19	0.67	21.6	14.4	36.0	7.2	530.0	7	7
JY-4	0.67	22.8	15.2	38.0	7.6	397.0	11	11
JZ-20	0.67	24.0	16.0	40.0	8.0	303.0	7	6
JM-20	0.67	25.0	16.6	41.6	8.4	109.0	9	8
JP-5	0.67	24.0	16.0	40.0	8.0	278.0	8	7
JO-4	0.67	26.0	17.3	43.3	8.7	60.0	14	13
JZ-19	0.67	27.0	18.0	45.0	9.0	23.0	8	7
JK-5	0.67	29.0	19.3	48.3	9.7	11.3	12	11
All specimens above are type A								
All specimens below are type B								
JN-5	1.64	15.5	25.4	40.9	9.9	795.0*	Corrected Elong.	
JW-10	1.64	16.0	26.2	42.2	10.2	308.0	Inch	Equiv. %
JO-9	1.64	16.5	27.1	43.6	10.6	67.7	.012	2.4
JP-11	1.64	17.0	27.9	44.9	10.9	44.2	.024	4.8
JV-15	1.64	18.0	29.5	47.5	11.5	23.5	.024	4.8
							.040	8.0
JX-10	∞	0	33.6	33.6	33.6	315.*	.001	0.2
JJ-10	∞	0	35.9	35.9	35.9	0.5	Grip Failure	
JT-13	∞	0	35.6	35.6	35.6	0.25	"	"
JO-5	∞	0	37.9	37.9	37.9	0.067	.001	0.2
JT-14	∞	0	38.8	38.8	38.8	0.033	.002	0.4
JV-14	∞	0	39.7	39.7	39.7	0.017	.005	1.0

* Test stopped before failure.

TABLE 3: TENSILE DATA for TITANIUM ALLOY at 1500° F and 1350° F

Specimen Number	Stress Ratio A	Applied Stress-KSI			Test. Temp. °F	Hours to Rupture	% Elongation	
		Mean	Alter	Crest			Uncor- rected	Cor- rected
V -23	0.	22.	0.	22.	1350	603.	4.0	3.0
V -20	0.	37.5	0.	37.5	1350	43.4	3.3	2.9
V -33	0.	45.	0.	45.	1350	15.8	4.6	4.3
V -26	0.25	23.	5.75	28.75	1350	747.	5.1	5.0
V -15	0.25	32.	8.1	40.1	1350	167.	3.7	3.6
V -12	0.26	36.	9.3	45.3	1350	40.4	2.5	2.5
V -11	0.25	40.	10.	50.	1350	34.8	3.4	3.2
V -14	0.26	42.	10.8	52.8	1350	25.	2.6	2.5
V -34	0.25	44.8	11.2	56.	1350	12.4	1.5	1.2
V -25	0.66	23.	15.3	38.3	1350	361.	1.35	1.35
V -22	0.66	27.	18.	45.	1350	185.	1.9	1.9
V -17	0.66	27.	18.	45.	1350	116.	1.7	1.6
V -7	0.68	30.	20.5	50.5	1350	132.	2.2	2.2
V -10	0.68	33.	22.5	55.5	1350	44.4	1.6	1.6
V -18	0.68	36.	24.4	60.4	1350	13.	1.3	1.0
V -24	0.	12.	0.	12.	1500	827.	2.15	2.12
V -21	0.	20.	0.	20.	1500	107.	2.5	2.2
V -19	0.	30.	0.	30.	1500	6.7	8.9	8.9
V -13	0.25	16.	4.	20.	1500	248.	1.9	1.8
V -6	0.25	20.	5.	25.	1500	109.1	2.9	2.7
V -5	0.25	24.	6.	30.	1500	54.9	5.3	4.0
V -4	0.26	24.	6.2	30.2	1500	13.	1.8	1.2
V -3	0.26	28.	7.2	35.2	1500	23.	5.5	4.9
V -9	0.25	32.	8.	40.	1500	7.0	4.3	4.0
V -16	0.67	15.	10.5	25.5	1500	229.	1.8	1.8
V -8	0.67	18.	12.	30.	1500	149.	1.8	1.7
V -1	0.68	22.5	15.2	37.7	1500	44.2	2.0	1.8
V -27	0.67	26.	17.3	43.3	1500	15.0	1.7	1.3
V -2	0.68	27.	18.2	45.2	1500	4.3	1.7	1.5

TABLE 4: TEST DATA for S-590 ALLOY at 1500° F and 1350° F

Specimen Number	Stress Ratio A	Applied Stress-KSI			Test Temp. °F	Hours to Rupture	% Elongation	
		Mean	Alter	Crest			Uncor-rected	Cor-rected
R5-11	0	22.0	0	22.0	1350	1753.	32.8	31.3
R5-2	0	26.0	0	26.0	1350	557.	26.6	26.0
R5-18	0	32.0	0	32.0	1350	60.2	35.4	35.3
R5-1	0	39.0	0	39.0	1350	15.5	25.9	25.5
R5-24	0.25	20.0	5.0	25.0	1350	4402.	10.9	10.5
R5-25	0.25	24.8	6.2	31.0	1350	484.	17.7	16.7
R5-4	0.25	32.0	8.0	40.0	1350	105.	31.6	31.
R5-13	0.25	40.0	10.0	50.0	1350	15.0	25.9	25.5
R5-17	0.67	22.0	14.6	36.6	1350	1578.	6.	6.
R5-29	0.67	24.0	16.0	40.0	1350	825.	12.	11.7
R5-7	0.67	30.0	20.0	50.0	1350	64.4	16.0	14.5
R5-14	0.67	33.0	22.0	55.0	1350	17.6	17.1	16.0
R5-10	0	12.0	0	12.0	1500	5137.	10.0	9.3
R5-8	0	17.0	0	17.0	1500	489.	10.3	9.0
R5-28	0	21.0	0	21.0	1500	104.	28.7	27.2
R5-3	0	27.0	0	27.0	1500	10.4	33.9	33.7
R5-20	0.25	10.0	2.5	12.5	1500	2900.*		
R5-27	0.25	14.0	3.5	17.5	1500	1847.	13.8	12.9
R5-5	0.25	22.0	5.5	27.5	1500	42.5	32.0	31.4
R5-16	0.25	25.6	6.4	32.0	1500	11.4	26.7	26.5
R5-23	0.67	12.0	8.0	20.0	1500	4119.	6.5	6.3
R5-30	0.67	14.0	9.3	23.3	1500	1786.	4.2	4.0
R5-9	0.67	22.0	14.6	36.6	1500	30.0	16.3	14.0
R5-19	0.67	24.0	16.0	40.0	1500	13.3	25.3	23.6

* Test stopped before failure.

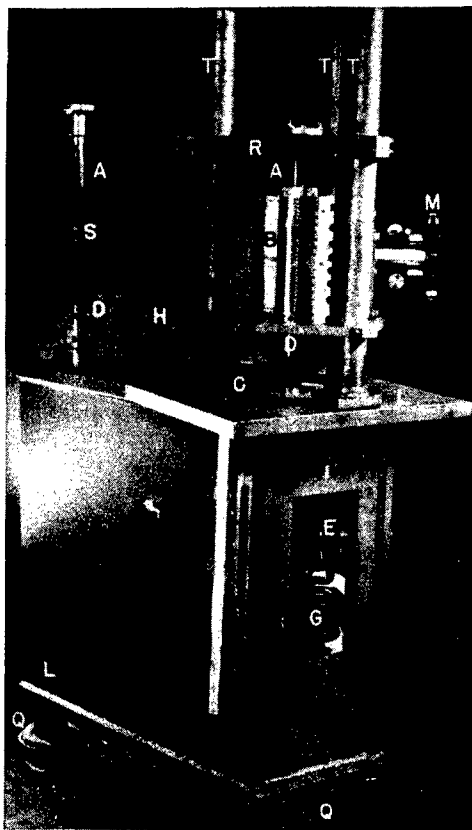


FIG. 1 PHOTOGRAPH OF DYNAMIC CREEP AND RUPTURE MACHINE

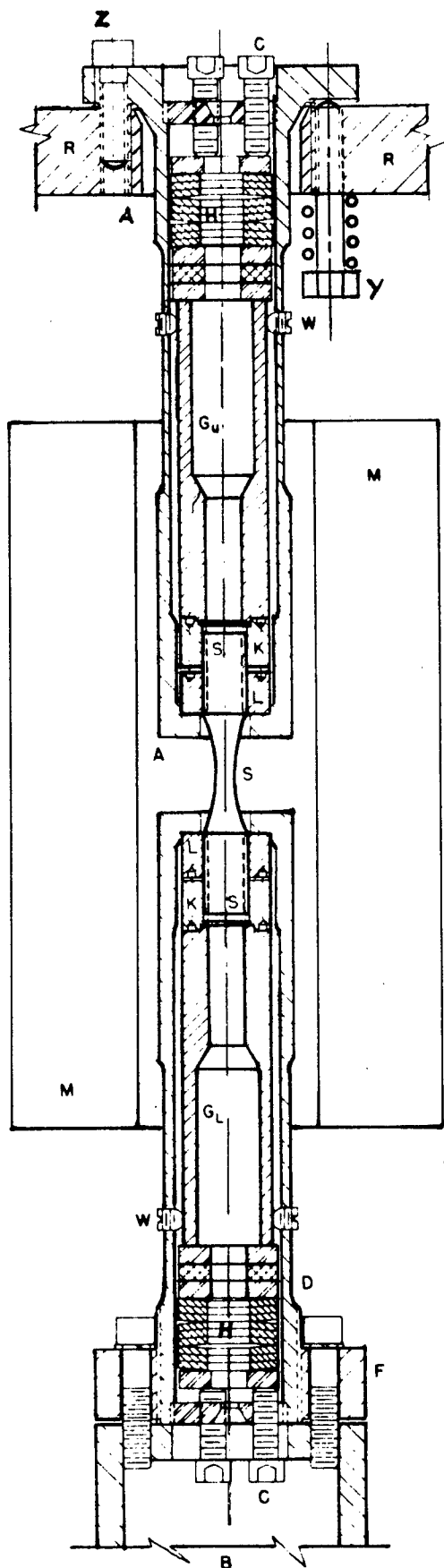


FIG 2 GRIP-SPECIMEN ASSEMBLY IN REVERSED STRESS FATIGUE TESTING

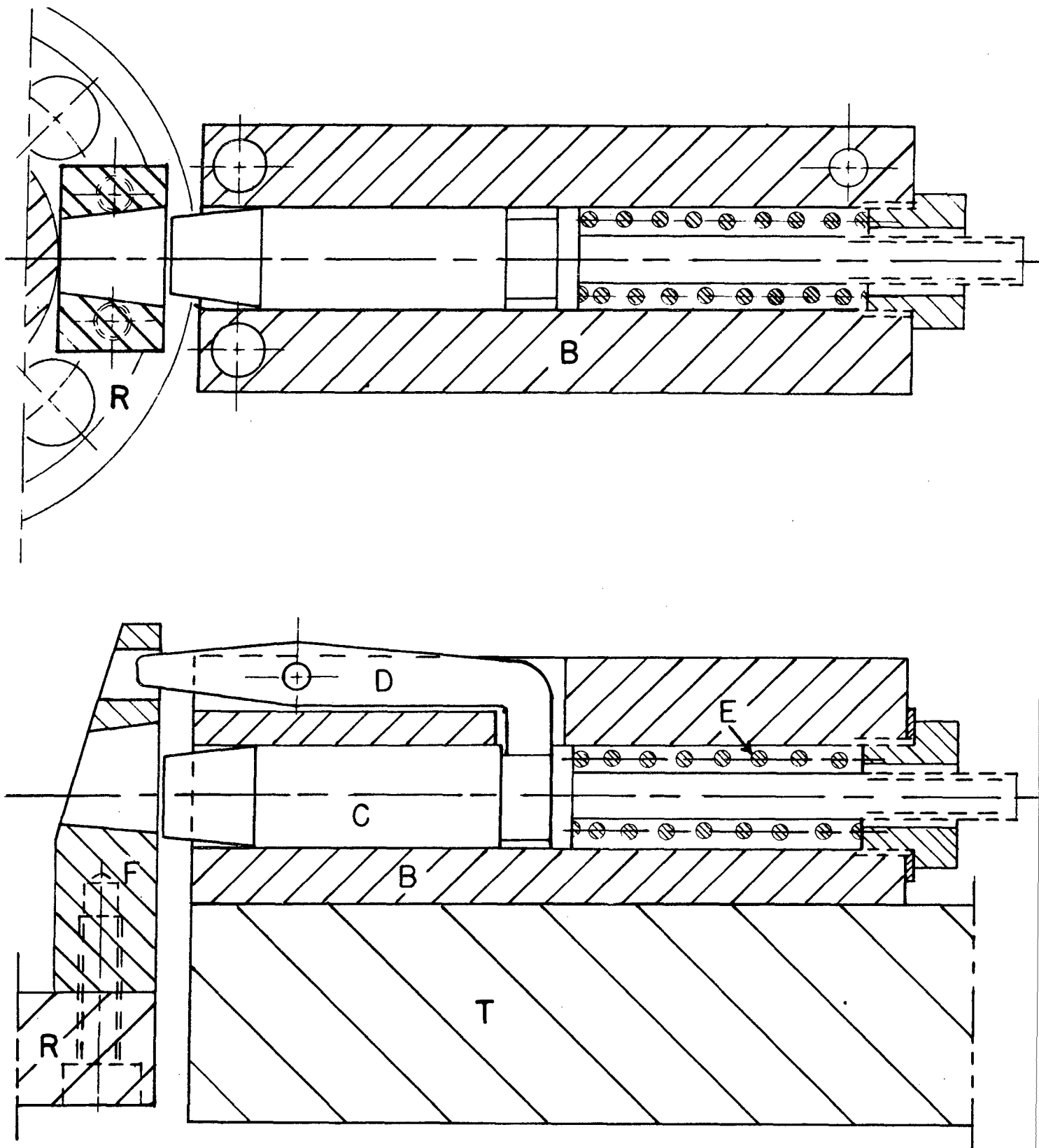


FIG. 3 SCHEMATIC DIAGRAM OF VIBRATION
LOCKING ATTACHMENT

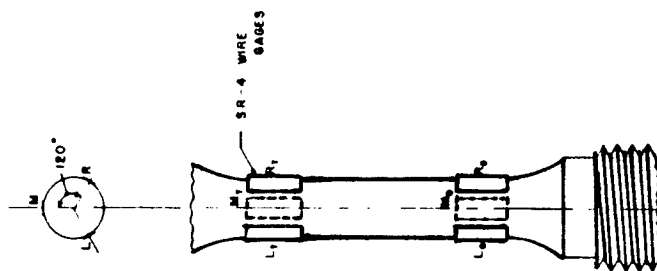


FIG 11 - Calibration Specimen
for Stress Distribution
Tests

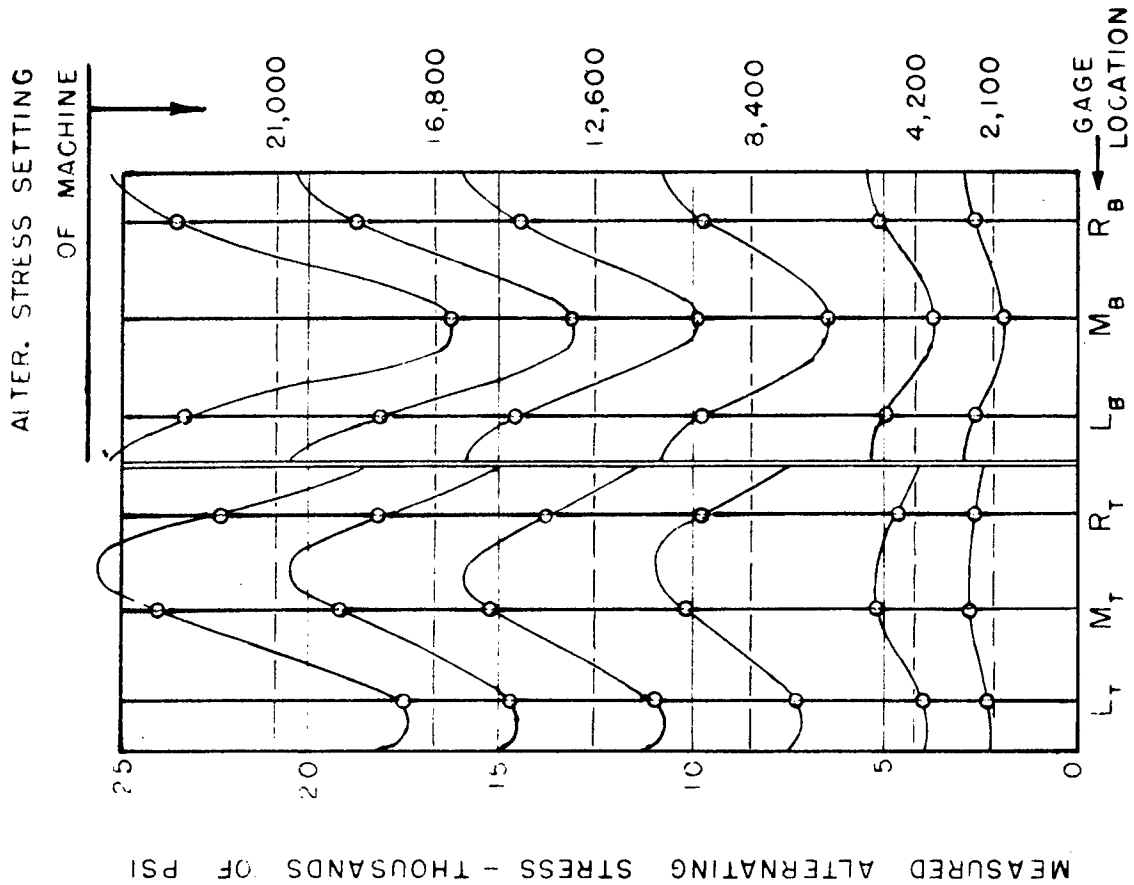
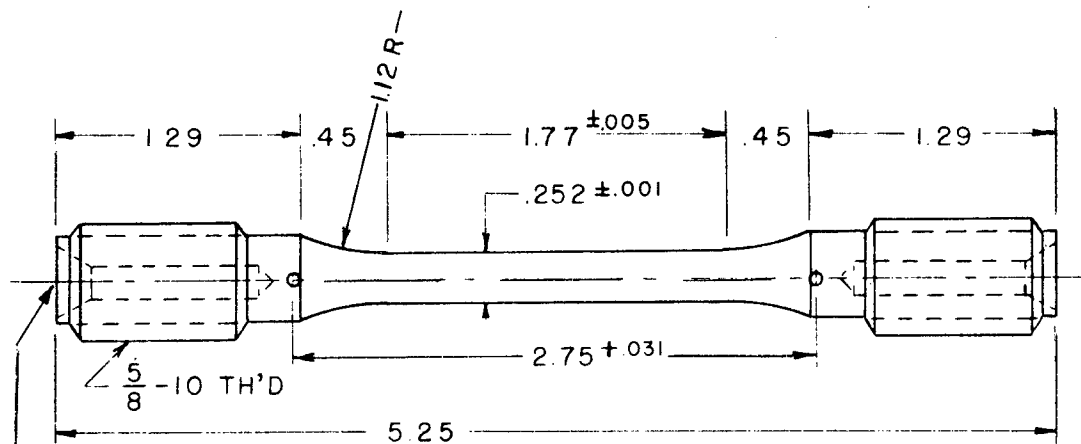
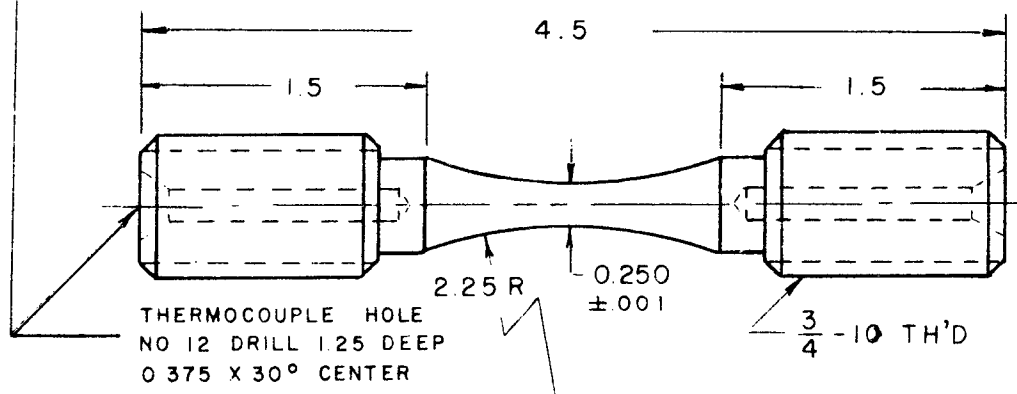


Fig 5 - Stress Distribution in Test Section of Specimen
Held by Early Version of Tension Compression Grip



TYPE A SPECIMEN FOR CREEP AND RUPTURE
TESTING UNDER AXIAL FATIGUE STRESS
IN TENSION RANGE



TYPE B SPECIMEN FOR FATIGUE TESTING UNDER
AXIAL STRESS IN THE TENSION-COMPRESSION
RANGE

FIG. 6 DRAWINGS OF DYNAMIC CREEP AND
RUPTURE SPECIMENS TYPE A AND B

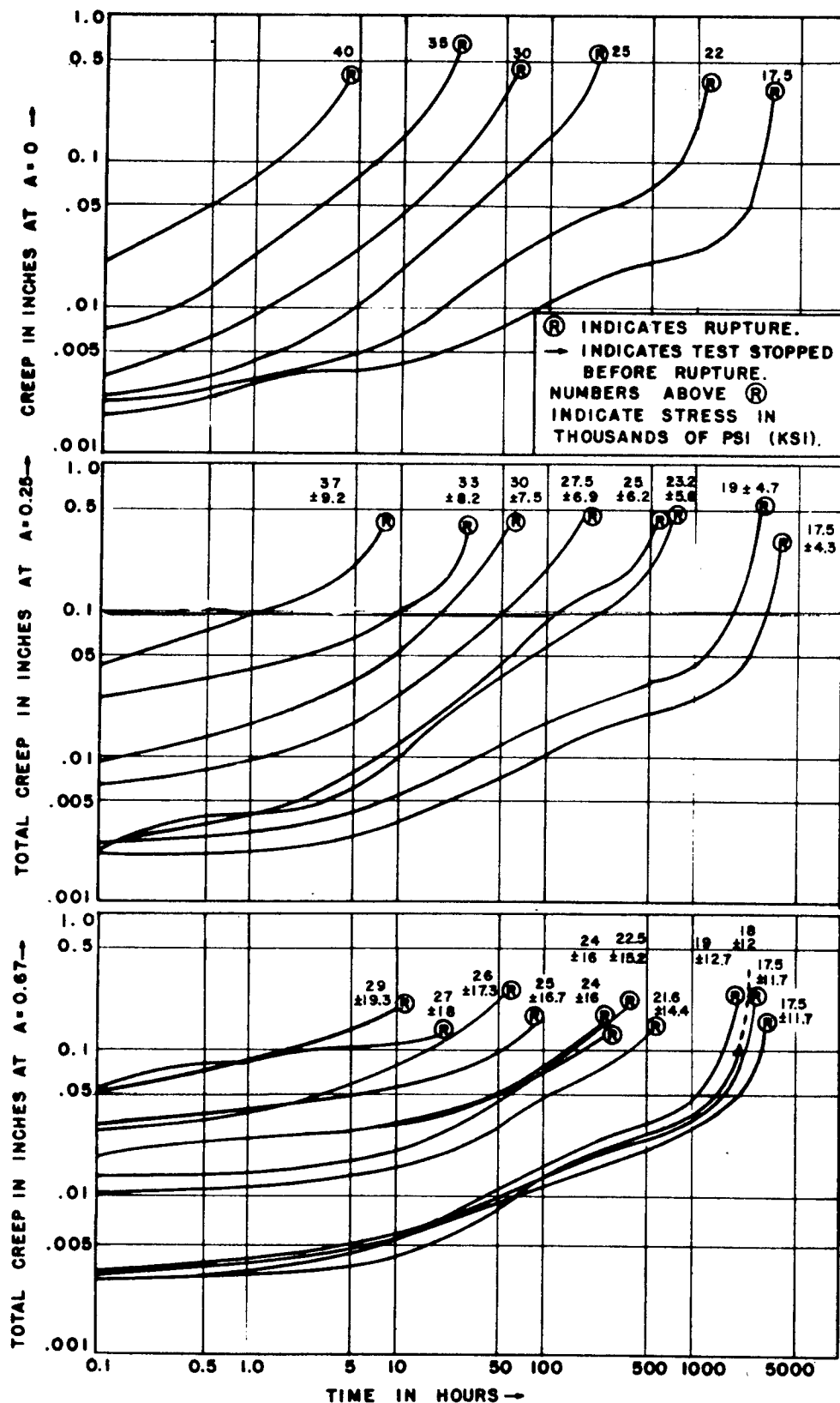


FIG. 7. TOTAL CREEP VERSUS TIME CURVES AT VARIOUS STRESSES AND STRESS RATIOS FOR N-155 AT 1350° F.

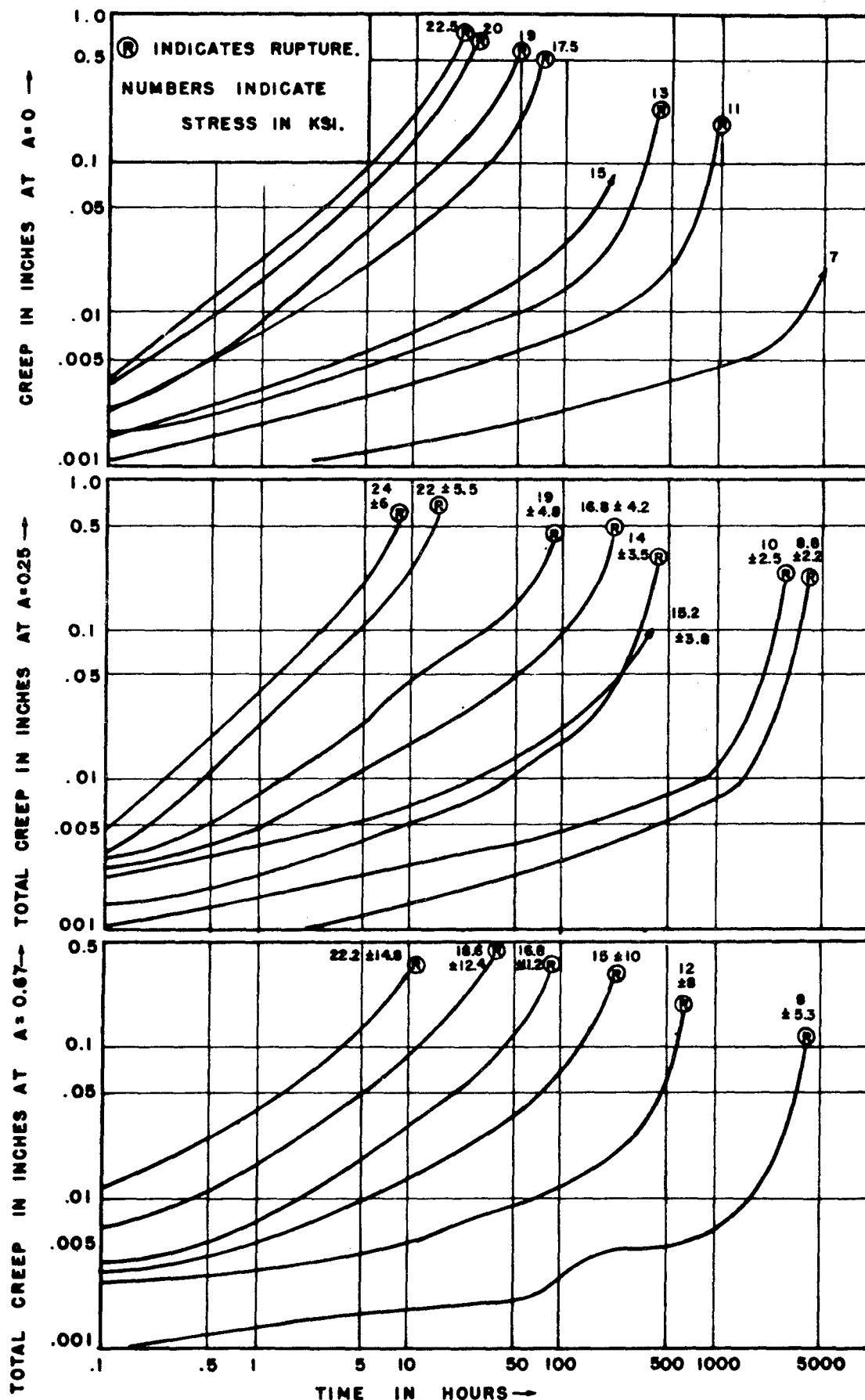


FIG. 8. TOTAL CREEP VERSUS TIME CURVES AT VARIOUS STRESSES AND STRESS RATIOS FOR N-155 AT 1500° F.

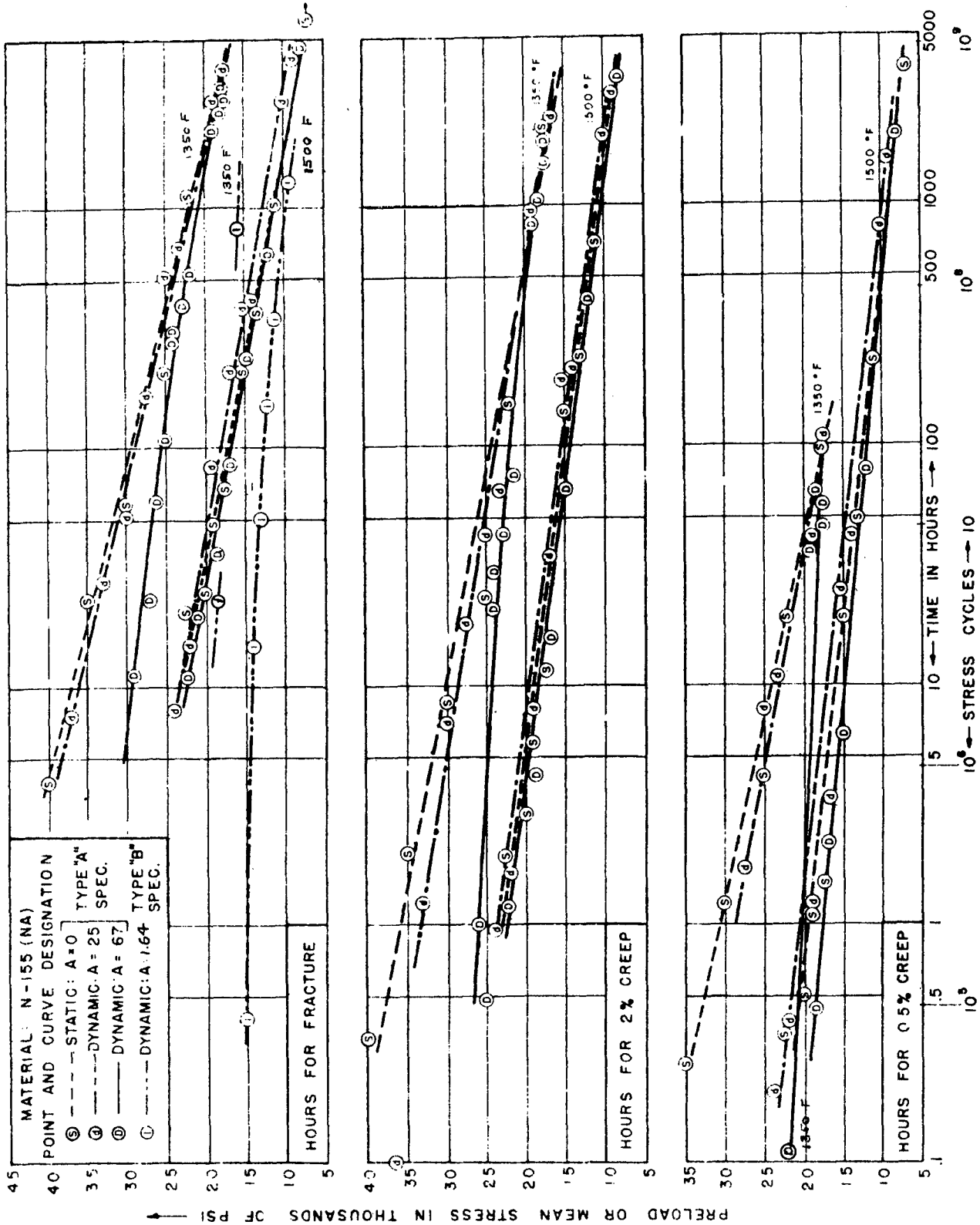


FIG. 9. TIME TO RUPTURE, 0.5% AND 2% CREEP VERSUS MEAN STRESS DURING THE STRESS CYCLE FOR N-155 AT 1350°F AND 1500°F.

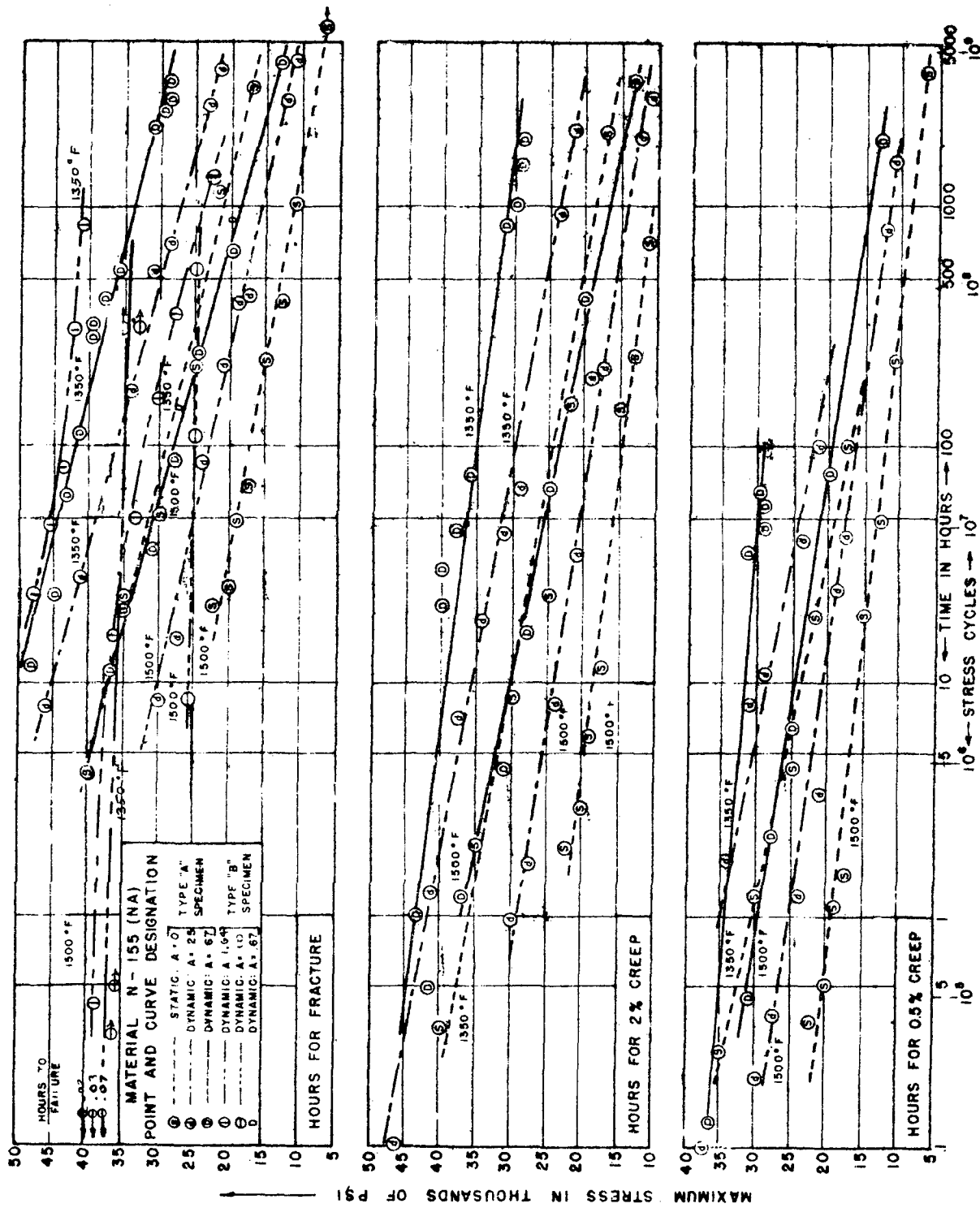


FIG. 10. TIME TO RUPTURE, 0.5% AND 2% CREEP VERSUS MAXIMUM STRESS DURING THE STRESS CYCLE

FOR N-155 AT 1350°F AND 1500°F.

S_A :- PRELOAD OR MEAN TENSILE STRESS IN THOUSANDS OF PSI →

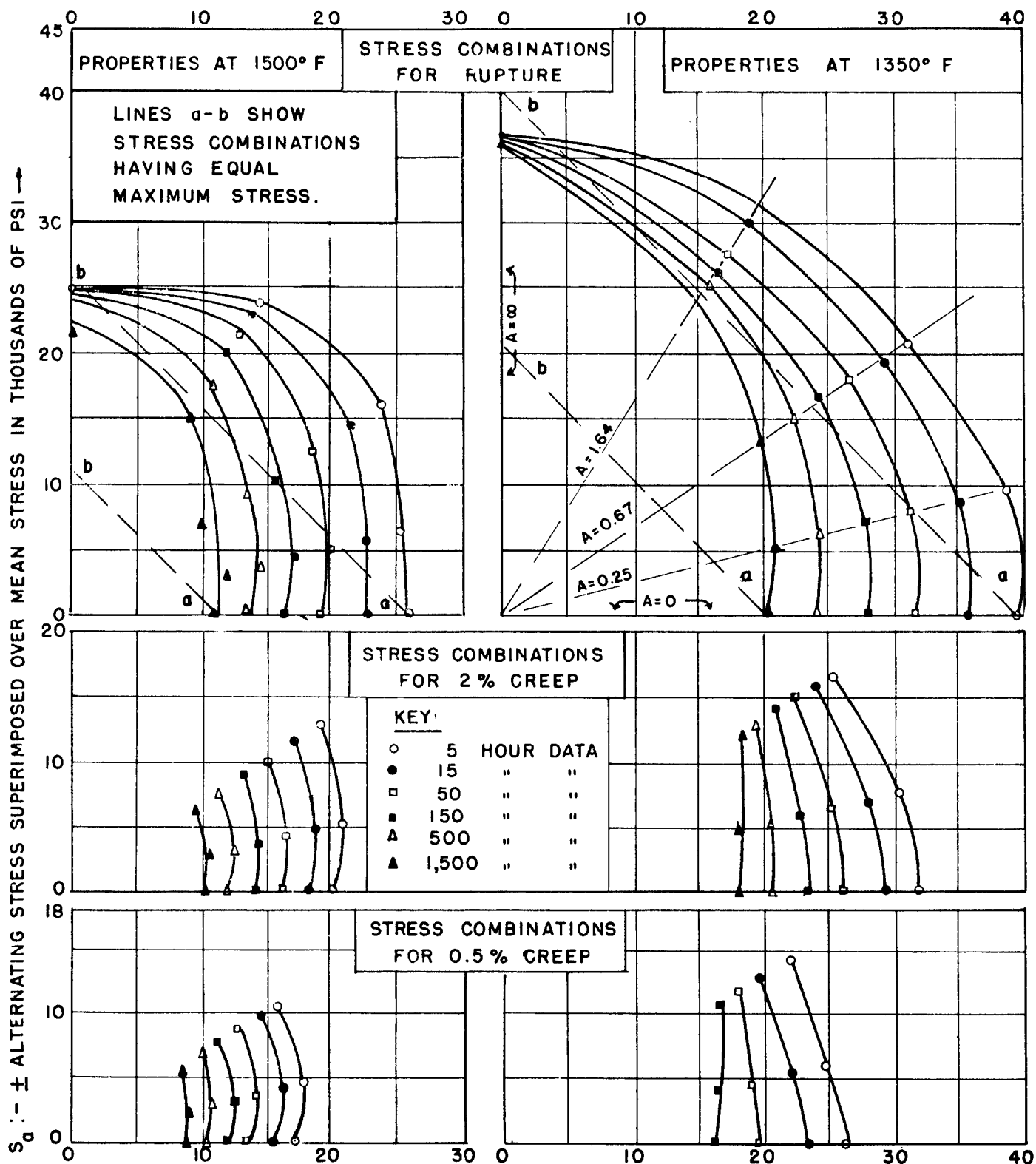


FIG.11. STATIC AND DYNAMIC STRESS COMBINATIONS WHICH CAUSE RUPTURE, 2% AND 0.5% CREEP IN HOURS INDICATED FOR N-155 AT 1500° F AND 1350° F.

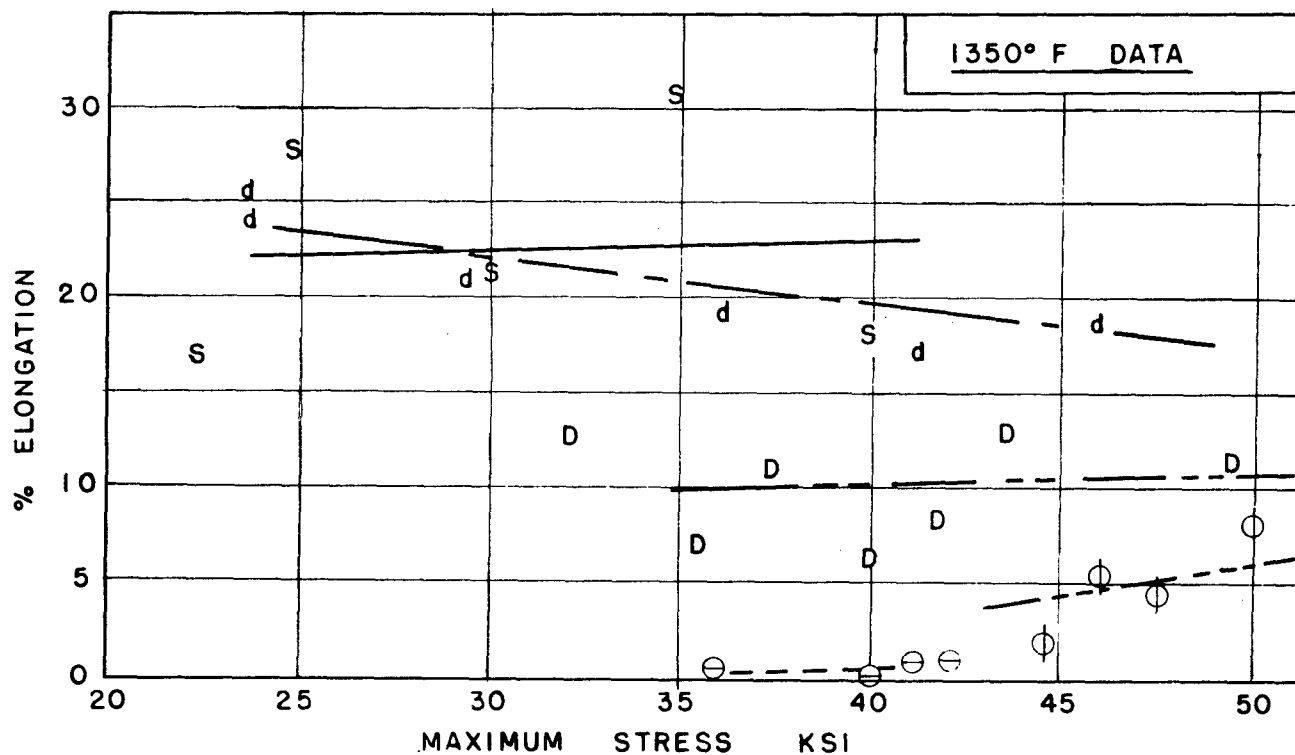
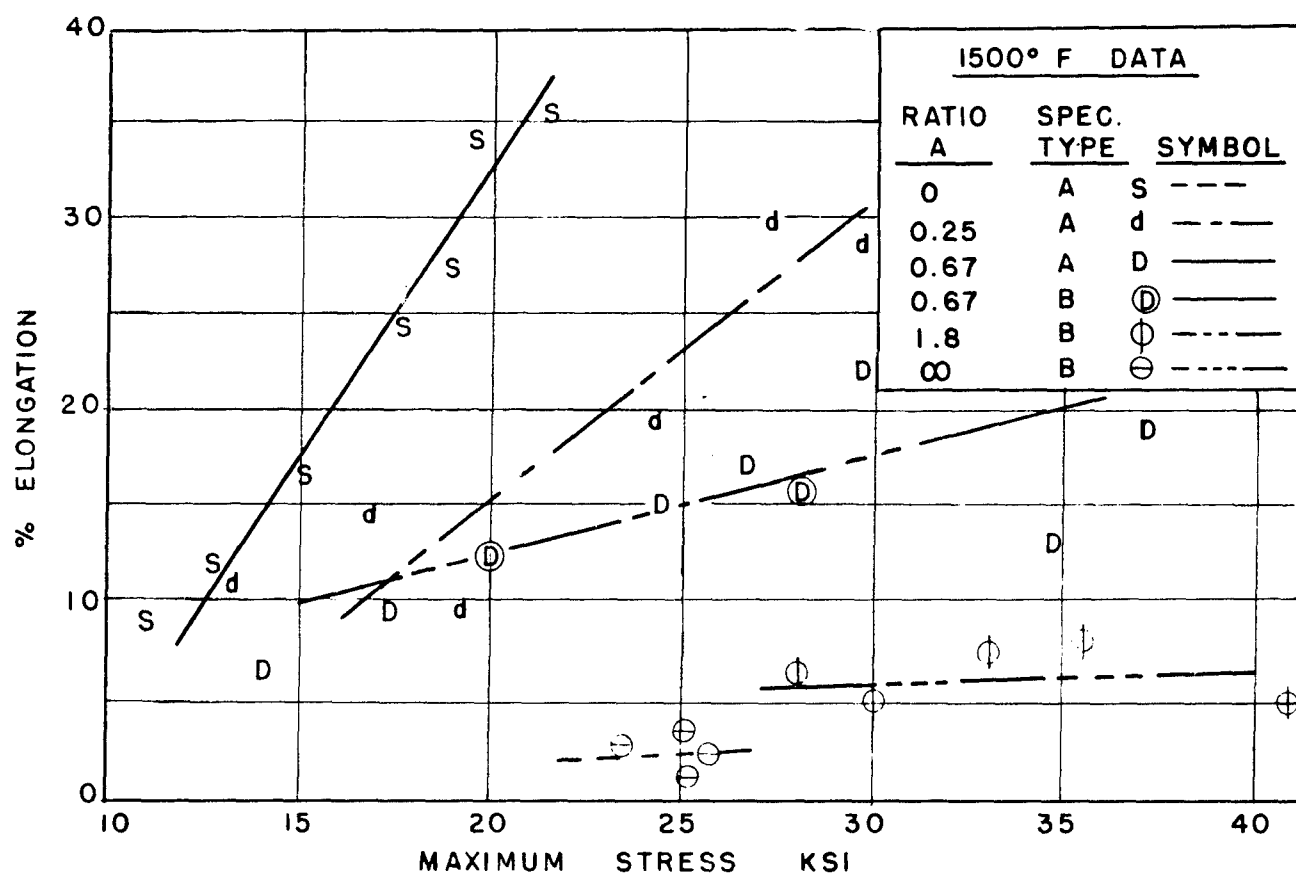


FIG. 12 EFFECT OF DYNAMIC STRESS RATIO A AND STRESS MAGNITUDE ON PERCENT ELONGATION OF ALLOY N-155 AT 1350 AND 1500° F.

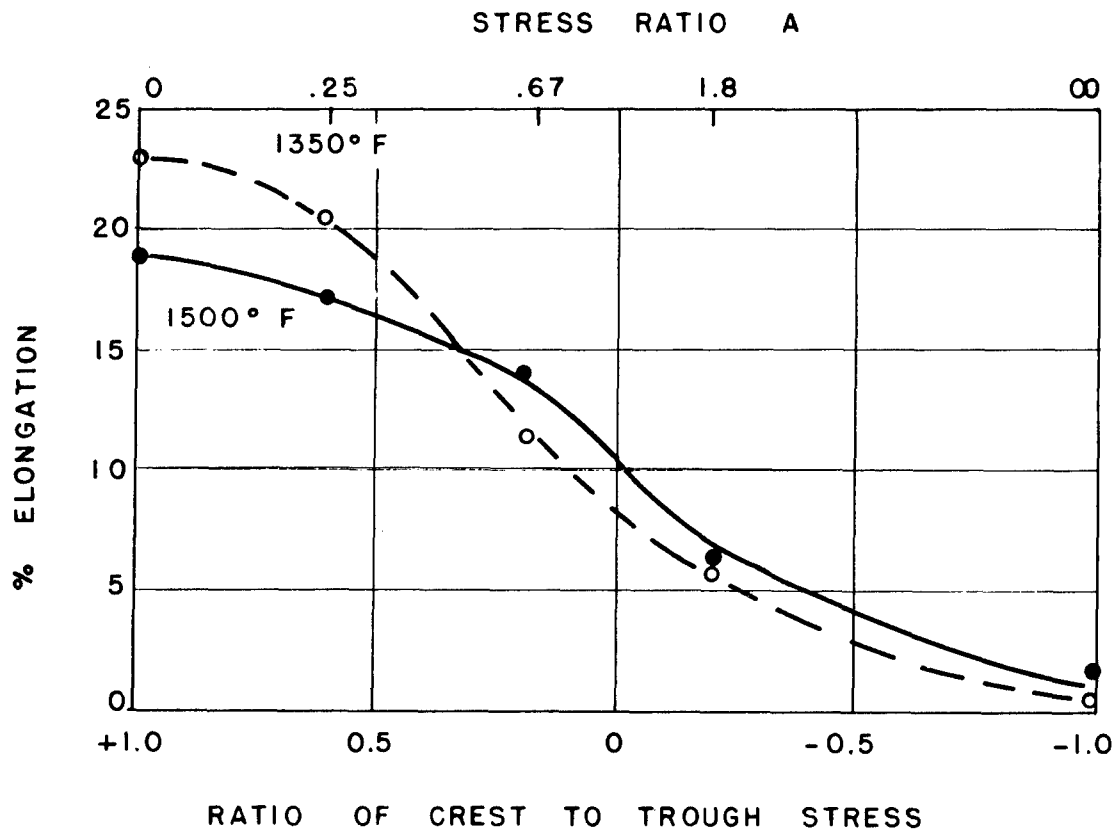


FIG. 13 EFFECT OF DYNAMIC STRESS RATIO
ON ELONGATION AT FAILURE IN 150
HOURS FOR ALLOY N-155 AT 1350
AND 1500° F.

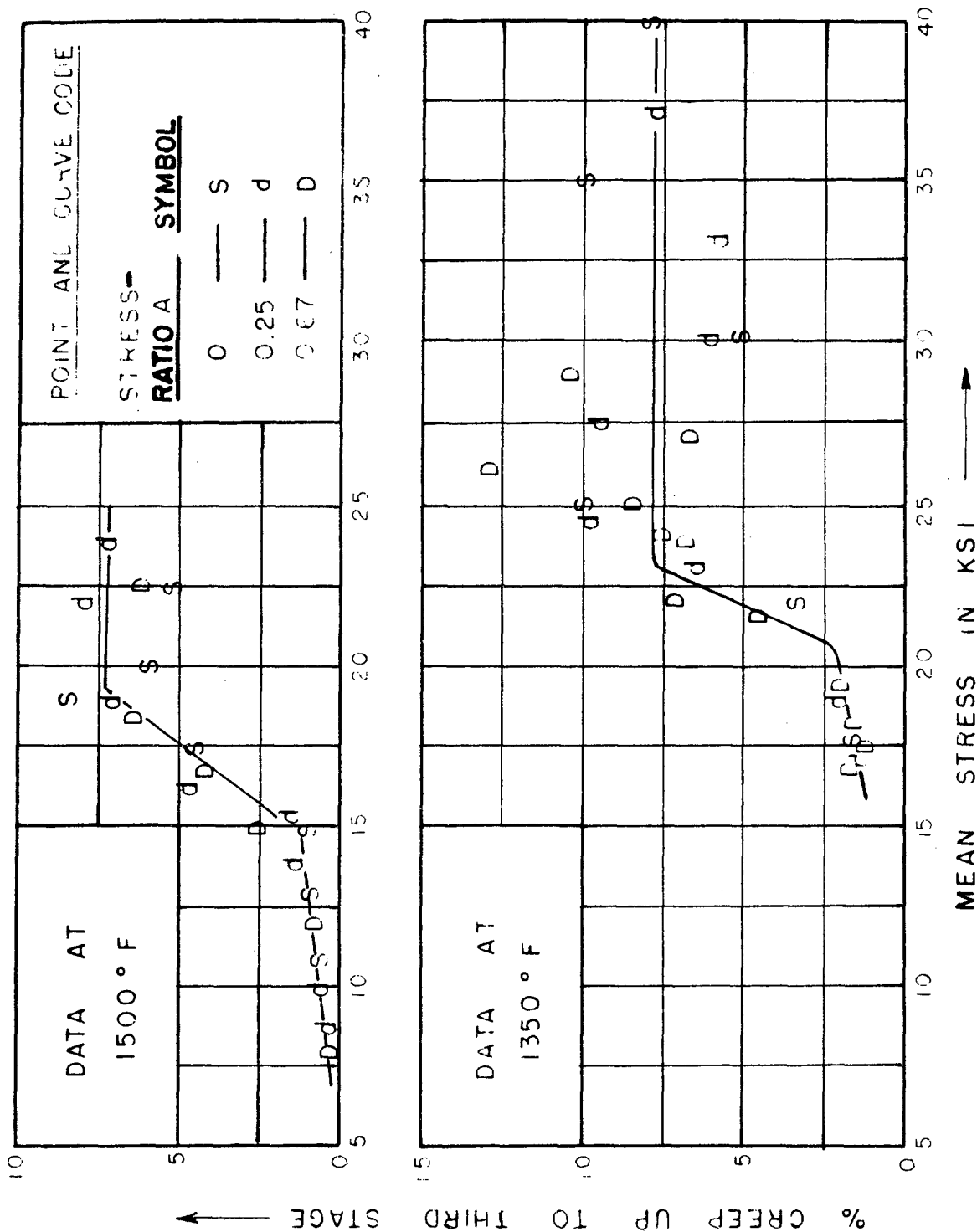


FIG. 14 EFFECT OF DYNAMIC STRESS RATIO AND MEAN STRESS ON % CREEP UP TO THIRD STAGE ON TYPE A SPECIMEN N-155

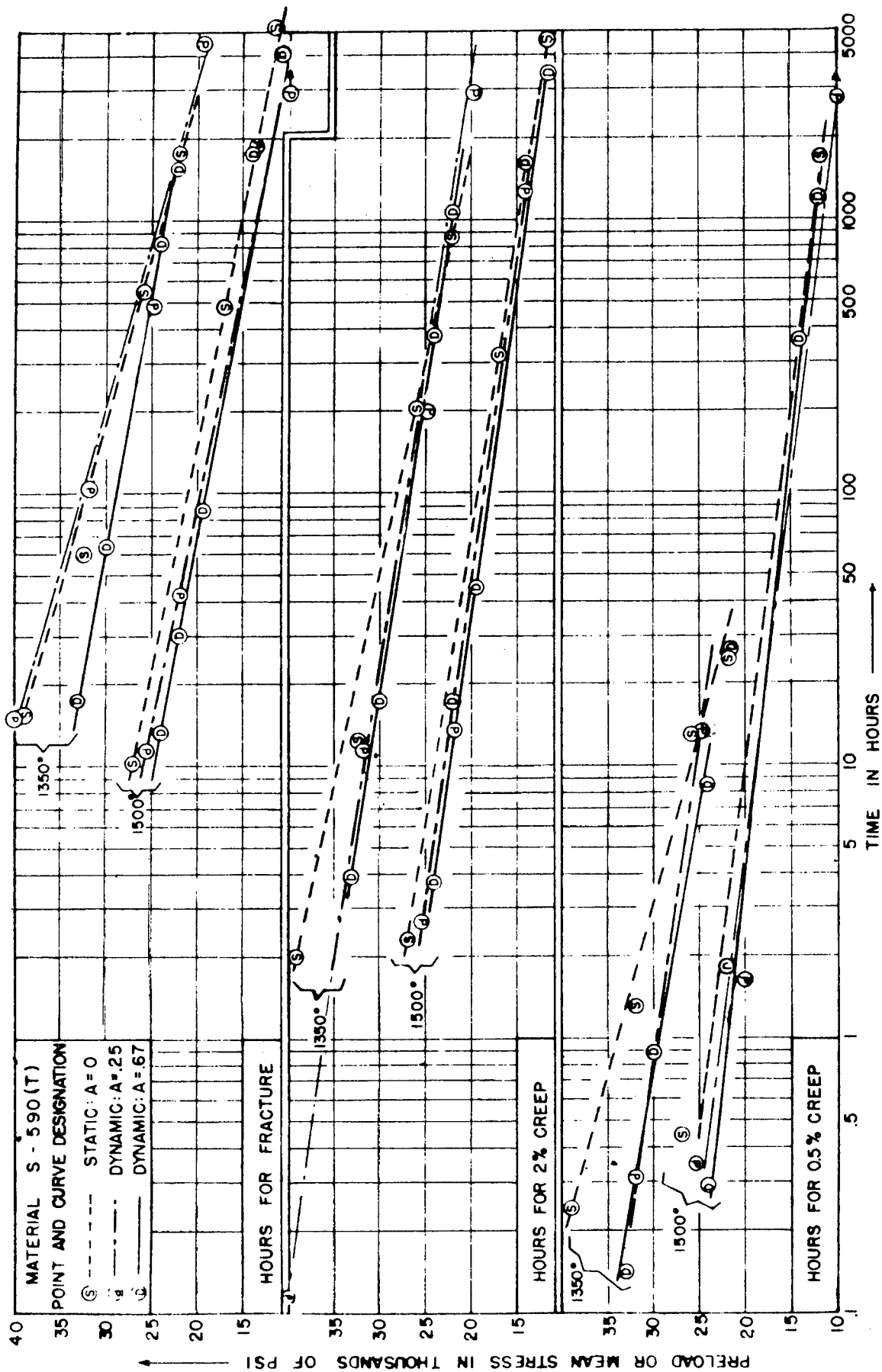
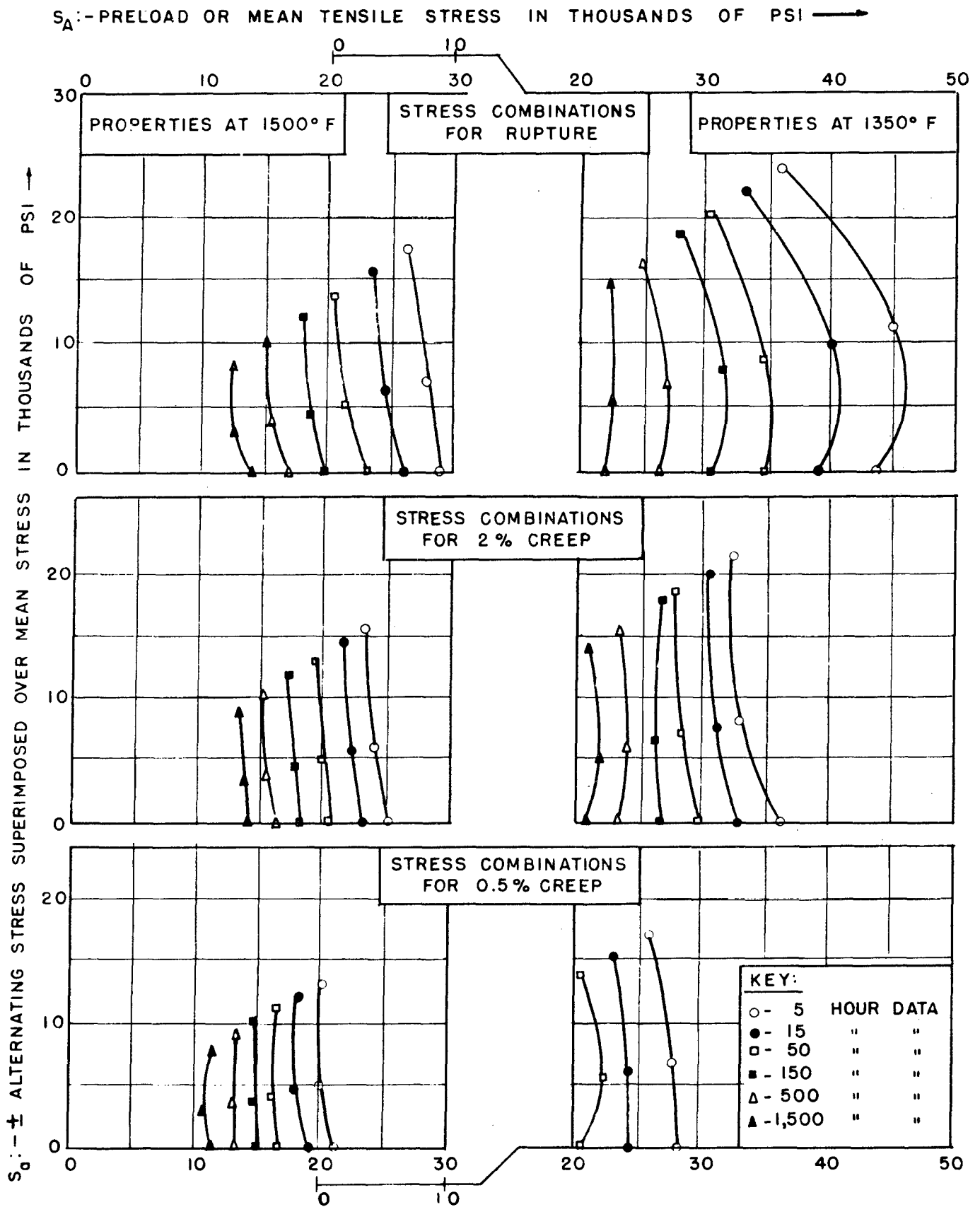


FIG 15. TIME TO RUPTURE, 0.5% AND 2% CREEP AT 1350°F AND 1500°F UNDER STATIC AND DYNAMIC TENSILE STRESS FOR S-590



S_m :-PRELOAD OR MEAN TENSILE STRESS IN THOUSANDS OF PSI →

FIG 16 STATIC AND DYNAMIC STRESS COMBINATIONS WHICH CAUSE RUPTURE, 2% AND 0.5% CREEP IN HOURS INDICATED FOR S-590 AT 1500° F AND 1350° F.

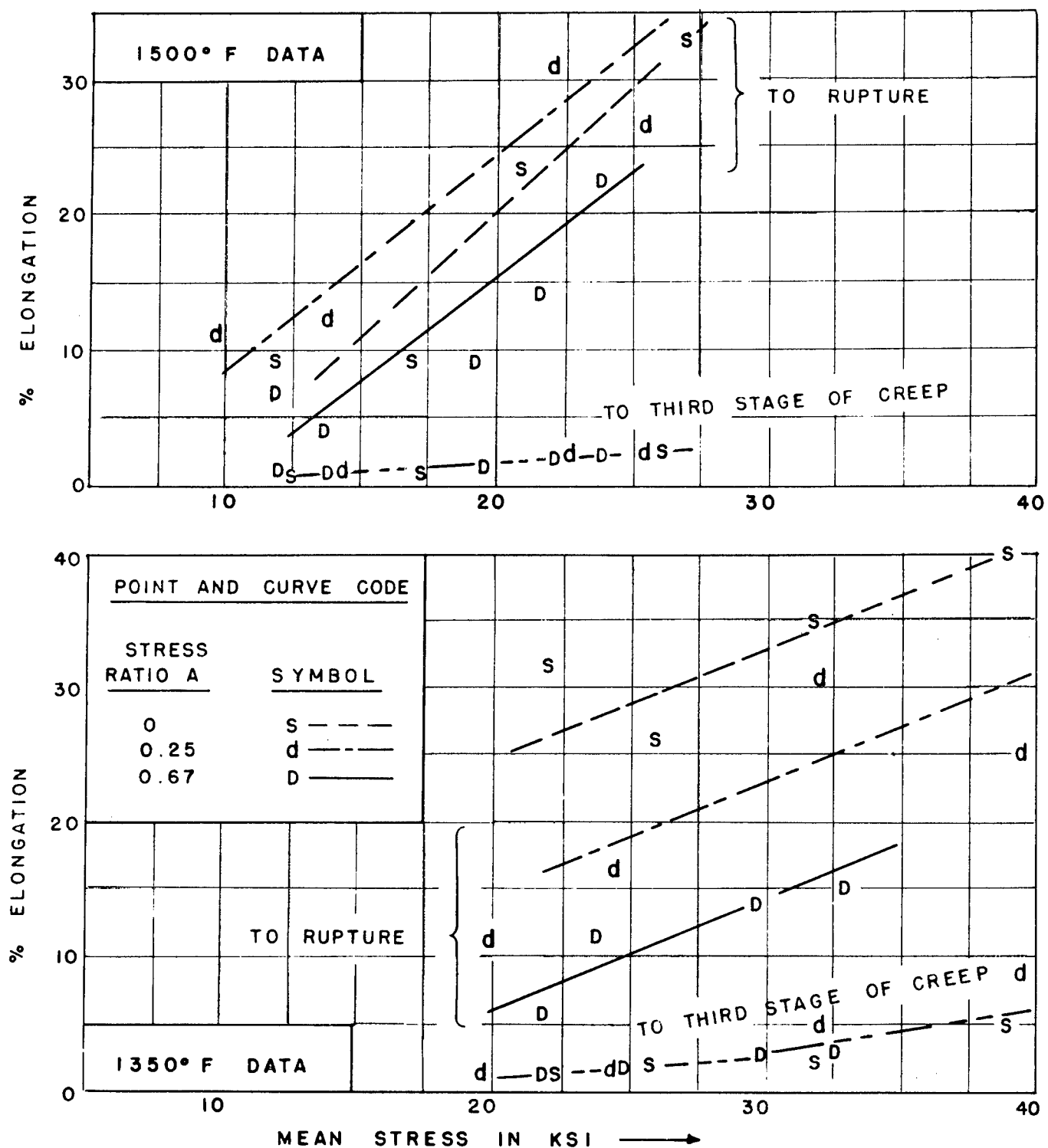


FIG. 17. EFFECT OF DYNAMIC STRESS RATIO AND MEAN STRESS ON PERCENT ELONGATION OF TYPE A SPECIMENS S-590.

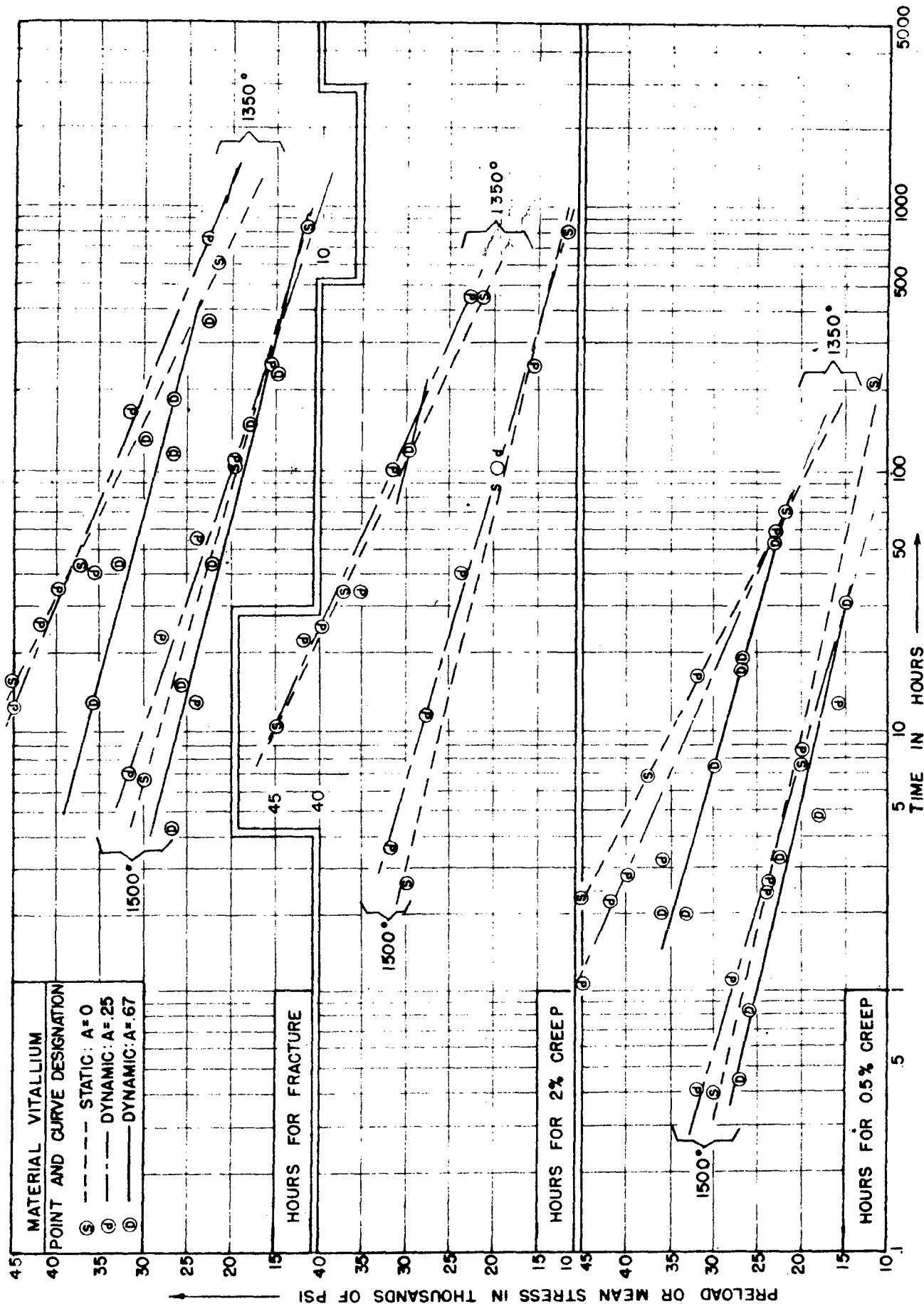


FIG 18. TIME TO RUPTURE, 0.5% AND 2% CREEP AT 1350°F AND 1500°F UNDER STATIC AND DYNAMIC TENSILE STRESS FOR VITALLIUM

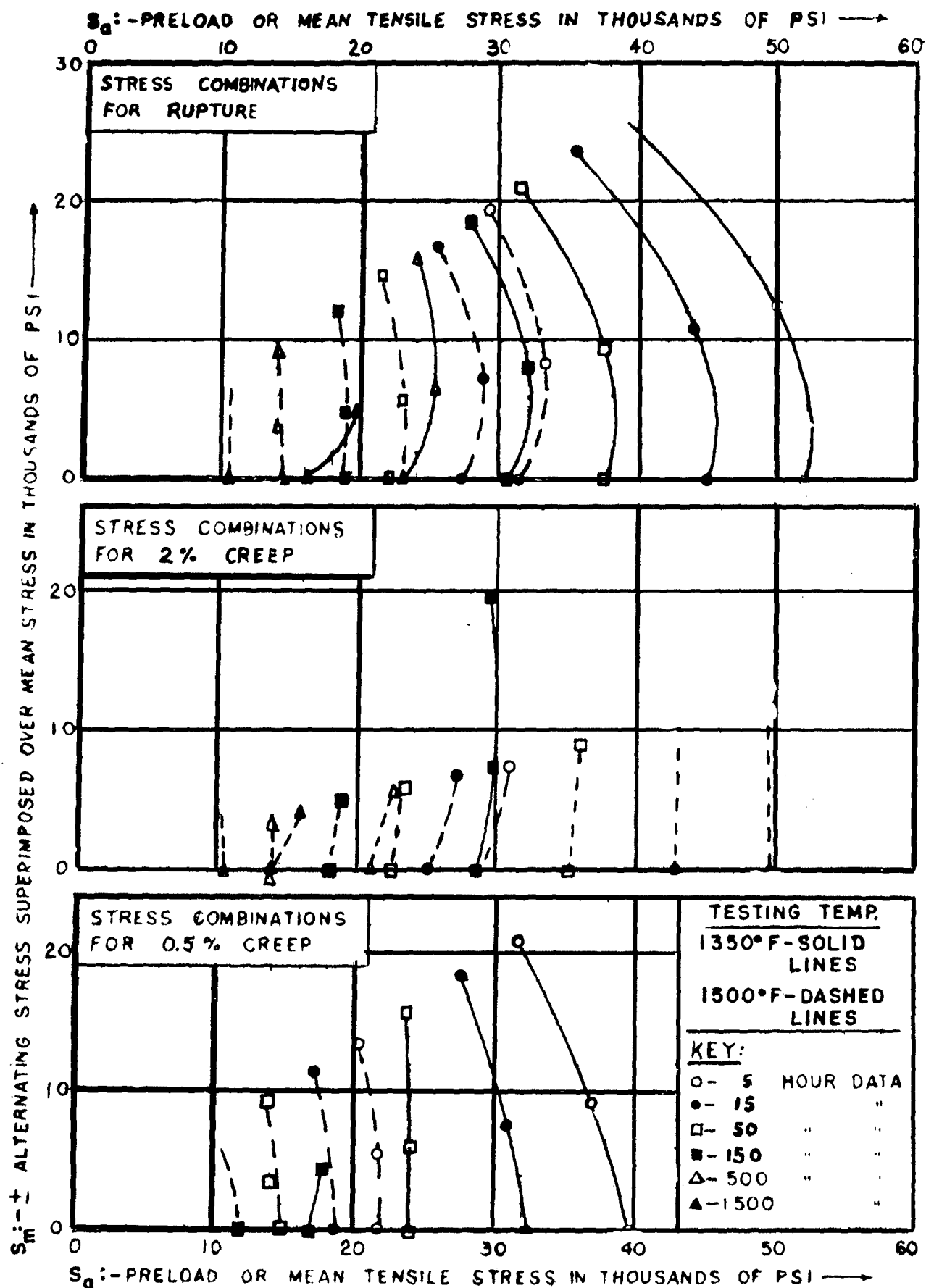


FIG. 19. STATIC AND DYNAMIC STRESS COMBINATIONS WHICH CAUSE RUPTURE, 2 % AND 0.5 % CREEP IN HOURS INDICATED FOR VITALLIUM AT 1350° AND 1500° F.

BIBLIOGRAPHY

1. I. Perlmutter and H. Adenstedt, "Service Failures of Turbine Buckets," AF Technical Report No. 5716, July 1948.
2. B. J. Lazan, "Dynamic Creep and Rupture Properties of Temperature Resistant Materials Under Tensile Fatigue Stress," Proc. Amer. Soc. for Test. Mater. Vol. 49, 1949.
3. N.A.C.A. Subcommittee on Heat-Resisting Materials "Cooperative Investigation of Relationship Between Static and Fatigue Properties of Heat-Resistant Alloys at Elevated Temperatures," NACA Report RM 51AO4, March 1951.
4. F. R. Morral, "Metallographic Studies on N-155 Specimens Exposed to Static and Dynamic Stress at Elevated Temperatures", Annual Report of February 1951 to Wright Air Development Center, WPAFB, Ohio, on Contract W 33(038)ac-15941 (to be issued as Air Force Technical Report).
5. B. J. Lazan and L. J. Demer, "Damping, Elasticity, and Fatigue Properties of Temperature Resistant Materials", ASTM Procedures, Vol. 51, 1951.
6. J. Marin, "Mechanical Properties of Materials and Design", page 134. McGraw Hill, 1942.